

# Evaluating the Total Human Electromagnetic Exposure in a UAV-aided Network

Thomas Detemmerman

Student number: 01707806

Supervisors: Prof. dr. ir. Wout Joseph, Prof. dr. ir. Luc Martens

Counsellors: Dr. ir. Margot Deruyck, German Dario Castellanos Tache

Master's dissertation submitted in order to obtain the academic degree of  
Master of Science in Information Engineering Technology

Academic year 2019-2020



## Acknowledgement

todo

# Contents

<b>List of Figures</b>	<b>viii</b>
<b>List of Tables</b>	<b>ix</b>
<b>List of Listings</b>	<b>x</b>
<b>Glossary</b>	<b>xi</b>
<b>Acronyms</b>	<b>xii</b>
<b>1 Introduction</b>	<b>1</b>
1.1 Outline of the Issue . . . . .	1
1.2 Objective . . . . .	2
1.3 Structure . . . . .	3
<b>2 State of the Art</b>	<b>4</b>
2.1 Deployment Tool for an UAV Network . . . . .	4
2.2 Electromagnetic Exposure . . . . .	5
2.2.1 Electromagnetic Field Radiation . . . . .	5
2.2.2 Specific Absorption Rate . . . . .	6
2.2.3 Related Work . . . . .	6

2.3	Optimizing towards electromagnetic exposure and power consumption . . . . .	7
2.4	Technologies . . . . .	7
2.4.1	Type of drone . . . . .	7
2.4.2	LTE . . . . .	8
2.4.3	Type of Antenna . . . . .	8
<b>3</b>	<b>Scenarios</b>	<b>11</b>
3.1	A single user . . . . .	12
3.2	Increasing traffic with only one drone available . . . . .	13
3.3	Increasing traffic with an undifend amount of drones . . . . .	14
<b>4</b>	<b>Methodology</b>	<b>16</b>
4.1	Electromagnetic exposure . . . . .	17
4.1.1	Calculation of the total specific absorption rate . . . . .	17
4.1.2	Electromagnetic exposure caused by far-field radiation . . . . .	17
4.1.3	Electromagnetic exposure caused by near-field radiation . . . . .	19
4.1.4	Defining an antenna . . . . .	21
4.1.5	Radiation pattern . . . . .	23
4.2	Optimizing the network . . . . .	25
4.3	Implementation . . . . .	26
4.3.1	Network planning, bringing it al together . . . . .	26
4.3.2	Implementation of the radiation pattern . . . . .	26
4.3.3	Performance improvement . . . . .	29
<b>5</b>	<b>Results and discussion</b>	<b>31</b>

5.1	Scenario 1: one user and one base station . . . . .	31
5.1.1	The influence from the maximum transmission power . . . . .	31
5.1.2	Influence of the flying height . . . . .	32
5.2	Scenario 2: increased traffic . . . . .	34
5.2.1	Influence of the flying altitude . . . . .	34
5.2.2	Influence of the number of users . . . . .	40
5.3	Scenario 3: . . . . .	44
5.3.1	Influence of the flying altitude . . . . .	44
5.3.2	Influence of the number of users . . . . .	47
<b>6</b>	<b>Conclusions</b>	<b>49</b>
	<b>Appendices</b>	<b>52</b>
<b>A</b>	<b>Radiation patterns: datasheet</b>	<b>53</b>
<b>B</b>	<b>Radiation patterns: example configuration</b>	<b>55</b>

## List of Figures

2.1	General design of a microstrip antenna . . . . .	9
4.1	Design of the microstrip patch antenna. . . . .	16
4.2	Distribution of how many phones belong to a certain SAR interval. Upper bound- ary not included . . . . .	21
4.3	Design of the microstrip patch antenna. . . . .	23
4.4	Radiation pattern 1: 3D model of the entire pattern on the left with the config- uration as described above. In the middle a 2D radiation pattern of the E-plane and at the right a 2D model of the H-plane. . . . .	24
4.5	Radiation pattern 2: Generated with a groundplane of 0.06m by 0.06m. On the left is the 3D model of the entire pattern plotted. In the middle a 2D radiation pattern of the E-plane and at the right a 2D model of the H-plane. . . . .	25
4.6	Schematic example of slices in a radiation pattern. . . . .	28
4.7	Schematic example of how bilinear interpolation works. . . . .	29
4.8	Example of a KD-three in two dimensions . . . . .	30
5.1	Minimal required transmission power by the antenna to reach the ground just below him. The red line shows the default maximum transmission power. . . . .	33
5.2	How SAR values from different sources are influenced by different flying altitudes	34
5.3	The influence of the flying height on the weighted average downlink exposure of users in the network. . . . .	35
5.5	Schematic overview of scenario 2 with only 2 users. . . . .	36

5.4	Scenario 2 with only 2 users. The coloured areas are only applicable for the orange user. The blue user is connected during the entire time. . . . .	36
5.6	The influence of the flying height on the total power consumption of the network.	37
5.7	This graph shows the percentage of covered users by one drone for different flying heights. . . . .	38
5.8	The influence of the flying height on the weighted average $SAR_{10g}$ of users in the network. . . . .	39
5.9	This figure shows how different sources are influenced by an increasing flying height. . . . .	40
5.10	The influence of increasing traffic on user coverage . . . . .	41
5.11	The influence of increasing traffic on user coverage . . . . .	41
5.12	The influence of increasing traffic on downlink exposure . . . . .	42
5.13	The influence of increasing traffic on the total power consumption . . . . .	42
5.14	This figure shows how different sources are influenced by an increasing number of users. . . . .	43
5.15	This figure shows how different sources are influenced by an increasing number of users. . . . .	44
5.16	The influence of the flying height on the downlink electromagnetic radiation of the average user. . . . .	45
5.17	This graph shows the percentage of covered users by one drone for different flying heights. . . . .	46
5.18	This graph shows how much drones are required for different flying heights while trying to achieve a 100% coverage. . . . .	46
5.19	The influence of the flying height on the total power consumption of the network.	47
5.20	The influence of the flying height on the weighted average $SAR_{10g}$ of users in the network. . . . .	48



## List of Tables

2.1	Specifications of the used drone. . . . .	8
3.1	Overview of default configuration values. . . . .	12
3.2	Overview of the configuration. . . . .	13
3.3	Overview of the configuration. . . . .	14
3.4	Overview of the configuration. . . . .	14
4.1	Overview of configuration parameters . . . . .	22
A.1	Overview of attenuation in dBm . . . . .	54

## List of Listings

1	Mathlab code to generate radiation pattern for a microstrip patch antenna . . .	24
2	Example configuration of a radiation pattern. . . . .	56

## Glossary

<b>equivalent isotropic radiator</b>	A theoretical source of electromagnetic waves which radiates the same intensity for all directions. 13, 14, 18, 26, 31, 32, 39, 41, 42, 44
<b>power flux density</b>	Magnitude of power ( $W$ ) that travels through a curtain area ( $m^2$ ). 19
<b>RRP</b>	RRP is an abbreviation used in this paper to indicate an extension on EIRP and stands for Real Radiation Pattern. An RRP value indicates the power (in dBm) for a certain location unlike an EIRP where the power (in dBm) is independent of the location. 18
<b>spurious radiation</b>	According to the thefreedictionary.com: Any emission from a radio transmitter at frequencies outside its frequency band. Also known as spurious emission. 9
<b>thermoregulatory capacity</b>	The capacity of an organism to regulate body temperture. 6

# Acronyms

<b>D/L</b>	downlink. 7, 8, 19, 25, 32, 37, 41, 42, 44
<b>EIRP</b>	equivalent isotropic radiation power. 12, 18, 34, 38
<b>FDD</b>	Frequency Division Duplex. 8
<b>ICNIRP</b>	International Commission on Non-Ionizing Radiation Protection. 5, 6
<b>IEC</b>	International Electrotechnical Commission. 20
<b>LOS</b>	line of sight. 18, 36
<b>LTE</b>	Long-Term Evolution. 8, 12, 19, 20, 31–33
<b>NLOS</b>	non line of sight. 36
<b>SAR</b>	Specific Absorption Rate. 6, 17, 20, 39, 43
<b>TDD</b>	Time Division Duplex. 8
<b>U/L</b>	uplink. 6–8, 17, 19, 21, 32, 44
<b>UABS</b>	Unmanned Aerial Base Station. 2, 4, 5, 7, 12–14, 17–19, 25–39, 41, 43, 44
<b>UE</b>	User equipment. 5, 12, 13, 17–20, 32, 39, 43, 44

# 1

## Introduction

### 1.1 Outline of the Issue

Society is constantly getting more and more dependent on wireless communication. On any given moment, in any given location, an electronic device can request to connect to the bigger network. Devices need more than ever to be connected, starting from small IOT sensors up to self-driving cars which all need to be supported by the existing infrastructure. Not surprisingly, the city center of Ghent has an average coverage of 97% of 4G over all telecom operators. [1]. Once again it becomes clear why we're on the eve of a new generation of cellular communication named 5G.

Also in exceptional and possibly life-threatening situations, the public relies on the cellular network. For example during the terrorist attacks at Brussels Airport, mobile network operators saw all telecommunications drastically increasing causing moments of contention. Some operators decided to temporarily exceed the exposure limits in order to handle all connections [2].

Electromagnetic exposure can however not be neglected. Research shows how excessive electromagnetic radiation can cause diverse biological side effects [3]. Because of public concern, the World Health Organization had launched a large, multidisciplinary research effort which

eventually concluded that there was no sufficient evidence that confirmed that exposure to low level electromagnetic fields is harmful [4]. A large part of the population remains nevertheless very concerned about potential health risks.

## 1.2 Objective

People are constantly getting exposed to several sources of electromagnetic radiation and it is important to consider this when designing a network. For this research, three prominent sources of radiation in a telecommunication network are investigated, being: the user's own phone, all base stations and all devices from other users in the network. In order to calculate electromagnetic exposure from all these sources, various parameters need to be known. Not only the used technology but also the position of the users and base stations are required. There are several publications discussing how the electromagnetic exposure originating from base stations can be calculated. Papers who cover electromagnetic exposure from all these different sources and convert it into a single value are rather limited.

To make this research possible, an existing planning tool is used which gives insight in user and base station distributions. The tool also provides information about path loss between radiators, power usage of the different electrical devices and which base station serve which user. In other words, the tool describes a fully configured network. In this way, all needed parameters will be known.

The electromagnetic behaviour of the network will be analysed by applying the tool in different scenarios to give insight which variables influence the exposure and how the network can be optimized accordingly.

**research question 1:** How can a Unmanned Aerial Base Station (UABS) network be optimized to minimize global exposure and overall power consumption? What are the effects on the network?

**research question 2:** What are the advantages and disadvantages of a model as described in research question 1 compared to the already existing path loss oriented model.

**research question 3:** How does the UABS fly height influence uplink and downlink exposure?

## 1.3 Structure

Related research to the subject is discussed in chapter 2: State of the Art, explaining electromagnetic exposure and its absorption into the body. Also the used technology such as type of antenna, type of base station and which infrastructure will be examined. The chapter also discusses why this master dissertation differs from other papers. Thereafter, chapter 3 talks about the different scenarios that will be investigated. Eventually, the methodology covers in chapter 4 the calculations and implementation of the different aspects excerpted in State of the Art. Chapter 5 shows the results of this implementation for the scenarios described in chapter 3. Finally, a conclusion of these results is formed in chapter 6.

# 2

## State of the Art

### 2.1 Deployment Tool for an UAV Network

Calculating electromagnetic exposure requires knowledge about the area. The position of base stations needs to be known, the transmission power used by the antenna and how far the user is separated from this base stations are only a few parameters that have to be considered.

The WAVES research group at UGent has developed a deployment tool for disaster scenarios with the aid of UAVs [5]. The idea of this UAV-aided emergency network is that in case of a disaster, the existing network might be damaged and won't be able to handle all users who are trying to reconnect to the backbone network. The tool makes a fast deployable network possible by attaching femtocells to UAVs, so-called UABSs. The tool will orchestrate the UABSs over the disaster area. This tool is thus a suitable starting point and works as follows:

The deployment tool will try to calculate the optimal placement for each UABS and requires therefore a description of the area where the UAV-aided network needs to be deployed. This is done with the use of so-called shape files. These files contain three dimensional descriptions of the buildings present in the area and are key values in approaching results as realistic as possible. Furthermore, the tool also requires a time period and a configuration file containing technical specifications of the type of UABS that is being used. The tool will thereafter ran-



domly distribute users over the area and assigns a certain bitrate to them.

In a second phase, the optimal position for each UABS is calculated. This is done by trying to locate a UABS above each active user. Two options are possible. If a fixed flying height is defined, a base station is placed above each user at the given height, unless a building is obstructing its location. Then, no base station will be located above that user. Alternatively to the fixed flying height, a flying margin can be defined which represents the distance between the outdoor user and the drone. If the user is inside, this margin will be measured between the drone and the rooftop of that building. The latter is only allowed if the suggested height remains below the given maximum allowed height.

Finally, all UABSs are sorted on whether they were active or not, followed by the increasing path loss from each UABS to that user. So the algorithm starts by checking for each active UABS if it can cover the user. If this is the case, the user will be connected to this UABS. If not, the second active base station with a (slightly) worse path loss is considered. If no active base station is suitable, inactive UABSs are considered. The user remains uncovered if no UABS is found. The reason behind only considering already active base stations at first, is the high cost that comes along with each drone.

Up till now, the tool has only calculated some suggestions. The actual provisioning is done in the fourth phase where drones are sorted by the amount of users they cover. As long as UABSs are available in the facility where they reside, UABSs are provisioned and its users are marked as covered.

## 2.2 Electromagnetic Exposure

### 2.2.1 Electromagnetic Field Radiation

People in a telecommunication network are exposed to far field electromagnetic radiation originating from base stations and other User equipment (UE). Network planners need to make sure that the electromagnetic fields (expressed in V/m) do not exceed limitations enforced by the government. These limits are location dependent. The European Union recommends the guidelines as defined by the International Commission on Non-Ionizing Radiation Protection (ICNIRP) which limits electromagnetic exposure to 61 V/m. Each European country needs to decide for themselves which limitations to enforce. Belgium for example delegated this responsibility to Flanders, Brussels and Wallonia [6].

The used deployment tool is applied in Ghent, a Flemish city in Belgium. The standards defined by the Flemish government are therefore applicable. They state that in the 2.6 Ghz frequency

band, an individual antenna can't exceed 4.5 V/m and the cumulative sum of all fixed sources has its maximum at 31 V/m.

### 2.2.2 Specific Absorption Rate

Specific Absorption Rate (SAR) represents the rate at which electromagnetic energy is absorbed by human tissue with the thermal effect as its most important health consequence. The volume of this tissue is typically 1 g or 10 g. The Federal Communications Commission of the United States defines regulations based on 1 g tissue (indicated as  $SAR_{1g}$ ) while the European Union handles the 10 g model ( $SAR_{10g}$ ). SAR values can further be categorized based on the area it covers. A first one is whole body SAR ( $SAR^{wb}$ ) which is the average absorbed radiation over the entire body. The second type is more precisely. Localized SAR-values cover only a part of the human body like the head. The ICNIRP has concluded that the threshold effect for  $SAR_{10g}^{wb}$  is at 4 W/kg meaning that any higher absorption rate would overwhelm the thermoregulatory capacity of the human body. Whole body values between 1 and 4 W/kg increase the temperature of human body less than 1°C, which is proven not to be harmful for a healthy human being[7]. Thereafter, a safety margin is introduced to tackle unknown variables like experimental errors, increased sensitivity for certain population groups and so on. This results in a whole body  $SAR_{10g}$  of 0.8W/kg and 2W/kg for localized  $SAR_{10g}$  at head and torso area [6].

### 2.2.3 Related Work

The goal of this master dissertation is the investigation of electromagnetic exposure considering all sources. Three types of sources are considered: electromagnetic radiation caused by base stations, near field radiation from the user's own device and far field radiation originating from other users' equipment. This electromagnetic radiation is thereafter absorbed by the human body which will be expressed in SAR values.

Several papers calculate exposure originating from certain sources, but very limited research has been done covering the whole picture. In [8] is described how electromagnetic radiation of several WiFi access points is being calculated. The authors of [9] used this knowledge to investigate electromagnetic exposure originating from base stations in a more outdoor environment. [10, 11] addresses the fact that also uplink (U/L) traffic from the user's device should be considered. They therefore investigated indoor exposure. They did not only consider the electromagnetic radiation but also how much is absorbed by the body, which will be expressed as specific absorption rate. Since the authors only covered voice calls, uplink SAR was expressed in localized SAR values while the downlink traffic is expressed in whole body SAR. With the advent of 5G, paper [12] has been published, describing how localized SAR values are achieved

from all sources. More precisely: all mobile phones and all base stations in the network after which they converted the electromagnetic exposure to localized SAR values. Finally, [13] describes how both U/L and downlink (D/L) traffic can be converted in whole body SAR values making it possible to achieve an overall picture. They applied this formula however only for the user's own device.

In a realistic network like the used deployment tool, some users are calling while others are using other types of telecommunication services like browsing the web. Therefore, all absorbed electromagnetic exposure should be expressed in whole body SAR while still covering all sources.

## 2.3 Optimizing towards electromagnetic exposure and power consumption

UABSs are drones with femtocell base stations attached to it. Drones can remain in the air for only a limited time, which is certainly the case when also an antenna needs to be connected to the battery of his carrier. It is therefore interesting to not only consider electromagnetic exposure of the user but also the power consumption that comes with it. However an increasing transmission power of an antenna comes with an increasing electromagnetic exposure. This is not the case considering both values for an entire network. In fact, the authors from [9] prove that both become inversely equivalent.

If a network is optimized towards power consumption, less drones will be provisioned radiating at higher power levels. This is because not only the transmission power is considered but also the power needed to keep the drone in the air. Therefore, it is cheaper to cover a user by increasing the antenna's transmission power of an already activated drone nearby as it therefore prevents the power cost of a new drone. By increasing the transmission power, also the electromagnetic exposure will increase for users closer to that drone. An exposure optimized network will therefore faster decide to power up a new drone.

## 2.4 Technologies

### 2.4.1 Type of drone

Section 2.1 described how femtocell antennae will be connected to helicopter drones. Two types of drones are considered in [5]: an off-the-shelf drone affordable by the general public and a more expensive drone. The results in [5] show that the second type will require less drones to cover the same number of users and will last longer in the air. The research in this paper will

therefore be done with the usage of the second type. A technical overview of this drone is given in table 2.1.

Parameter	value
Carrier power	13.0 A
Average carrier speed	12.0 m/s
Average carrier power usage	17.33 Ah
Carrier battery voltage	22.2 V

Table 2.1: Specifications of the used drone.

### 2.4.2 LTE

The tool makes usage of Long-Term Evolution (LTE), by the general public better known as 4G. LTE allows better U/L and D/L data speeds compared to its predecessors and is based on an all IP architecture. This technology can cover macrocells supporting cell sizes ranging from 5 km up to 100 km. These types of antennae are usually attached to transmission towers along highways or on top of buildings. LTE supports however also smaller cells like femtocells covering only a few hundred meters. They are therefore more portable, require less energy and won't require a telecommunication operator because of their simplicity. Femtocell base stations are therefore used by the deployment tool. Further, LTE also support both Frequency Division Duplex (FDD) and Time Division Duplex (TDD).

FDD makes simultaneous U/L and D/L traffic possible by assigning different frequencies within the frequency range to both data streams. A small guard band is used between the U/L and D/L direction in order to prevent interference.

TDD allows U/L and D/L traffic by splitting the time domain. Meaning that both traffic directions use the same frequency and therefore alternately (in time) use the same frequency. A small time interval is used to prevent interference in case of a slightly bad timed synchronization.

This master dissertation will make usage of FDD.

### 2.4.3 Type of Antenna

An important part of this master dissertation is the type of antenna that will be used by the femtocell base stations. The deployment tool makes use of drones that will position the femtocell base stations in the right position. Using conventional sector antennae, as used by traditional terrestrial transmission towers, would be too complicated for a simple drone. The characteristics of microstrip antennae will therefore be investigated.

Microstrip antennae provide several advantages compared to traditional antennae [14, 15]. Microstrip antennae are lightweight, low in cost and thin causing them to be more aerodynamic which is a useful feature since the antennae will be attached to flying drones.

A basic microstrip antenna like figure 2.1 consists of a ground plane and a radiating patch, both separated with a dielectric substrate. Several variations exist like microstrip patch antenna, microstrip slot antenna and printed dipole antenna which all have similar characteristics. They are all thin, support dual frequency operation and they all have the disadvantage that they will transmit at frequencies outside the aimed band which is also known as spurious radiation. The microstrip patch and slot antenna support both linear and circular polarization while the printed dipole only supports linear polarization. Further is the fabrication of a microstrip patch antenna considered to be the easiest of its competitors [14].

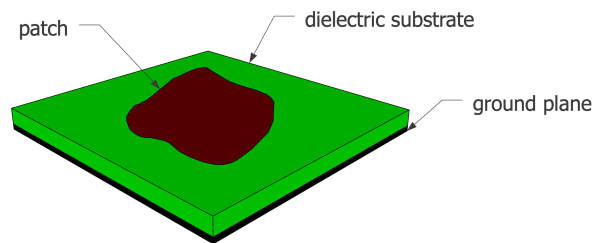


Figure 2.1: General design of a microstrip antenna

The microstrip antenna requires besides the groundplane, dielectric substrate and the radiation patch also a feed line. Several feeding techniques exist of which the most popular are: coaxial probe feeding, microstrip line and aperture coupling.

A first feeding method is with the usage of a coaxial cable where the outer conductor is attached to the ground plane and the inner conductor to the radiations patch. Modelling is however difficult, especially for thick substrates as will be used in this master dissertation. A second option is the usage of a microstrip line. This type of feeding is much easier to model since the microstrip line can be seen as an extension of the radiating patch. A disadvantage is the increased spurious radiation which limits bandwidth. A third is proximity coupling which has the largest bandwidth and low spurious radiation. It consists however of two dielectric substrates causing the overall thickness of the antenna to increase as well as its fabrication difficulty.

The increasing usage of the microstrip patch antennae can be explained by its easy fabrication and light weightness and therefore knows a widespread application in the military, global positioning systems, telemedicine, WiMax applications and so on. The authors of [16] also state that some of the disadvantages like lower gain and power handling can be solved with the usage of an array configuration.

The radiating patch is usually made of a thin layer of either gold or copper [15, 17] and can have any form. However, shapes other than circles or rectangles would require large numerical computation [15]. A simple rectangular shape will thus be used. Further, also the dielectric constant of the substrate is important. It typically varies between 2.2 and 12. Finding a good dielectric depends on how the antenna will be used. A lower dielectric constant with a thick substrate will result in better performance, better efficiency and larger bandwidths [17]. On the other hand, a larger dielectric constant reduces the dimensions of the antenna [15] which is also useful when attaching the antenna to a limited surface. Glass as a dielectric substrate with a constant of 4.4 will be used.

# 3

## Scenarios

The tool supports multiple configurations and the behaviour will be different for most these configurations. Three main scenarios will be investigated, order based on the network complexity. Within each scenario, different configurations will be applied. For the first scenario, only one user with one drone will be present in the network. The network will thereafter be expanded for multiple users but with still only one drone available. Eventually, that last restriction will be dropped meaning that the third scenario covers multiple users with unlimited number of drones. Table 3.1 show the default configuration which values are always applicable unless mentioned otherwise.

<b>Broadband cellular network</b>	
technology	LTE
frequency	2.6 GHz
<b>Carrier</b>	
carrier power	13.0 A
average carrier speed	12.0 m/s
average carrier power usage	17.33 Ah
carrier battery voltage	22.2 V
<b>Femtocell antenna</b>	
maximum $P_{tx}$	33 dBm
antenna direction	downwards (az: 0°; el: 90°)
gain	4 dBm
feeder loss	2 dBm
implementation loss	0 dBm
radiation pattern	EIRP or microstrip patch antenna
height	100m
<b>UE Antenna</b>	
height	1.5m from the floor
gain	0 dBm
feeder loss	0 dBm
radiation pattern	EIRP
number present in the network	224

Table 3.1: Overview of default configuration values.

### 3.1 A single user

This first scenario will investigate how  $SAR_{10g}$  and power consumption is influenced in an isolated environment meaning there is no influence from other base stations nor other UE. The tool will provision one single drone and position it directly above the user. These results will however depend on the position of the user. If the randomly generated location of the user is indoor, the flying height of the drone might be obstructed by the building where the user resides, causing the user to be uncovered. If this is not the case, the expected altitude of the user is half of the height of the building meaning that the user would be closer to the UABS as if he would have been outdoors. For a more consistent result, the user will therefore be positioned outside when systematically increasing the flying height.

Another considered variable will be the transmit power of the antenna. LTE makes use of power control meaning that no more power will be used than strictly necessary. The actual



transmit power therefore ranges between 0 and the maximum input power. This power is zero when either no user is present or the user is so far away that the actual transmit power would exceed the maximum transmission power. Increasing the maximum transmission power won't influence the power consumption or  $SAR_{10g}$  because the UABS won't use more than strictly required. It is therefore more useful to match the actual transmit power against a variable flying height.

This scenario investigates  $SAR_{10g}$ , power consumption and minimal transmission power. The used optimization strategy is not important. The optimization algorithm decides which user will be connected to which drone in order to reach a certain goal. Since only one user and one UABS are available, both optimization strategies will behave identical. These values will be checked when using a fictional equivalent isotropic radiator and a realistic antenna.

The user gets a fixed position. The exact location doesn't matter as long as it is outside. For this experiment is chosen for the 'Koningin Maria Hendrikaplein', a square just next to the train station of Ghent. Doing so will force the UE to always be at the same height of 1.5 meters. The conclusions will be based on  $SAR_{10g}$ , power consumption and transmission power. These output values depend on fly height and type of antenna. An overview can be found in table 3.2

Note that there is no explicit restriction on the number of drones in table 3.2. The deployment tool initially places UABSs above each user and it is the optimization strategy that decides which of these potential positions remain. Since there is only one user, there can also be only one drone.

Parameter	Value	Input variables	Output variables
x position user	3.711198	type of antenna	$SAR_{10g}$
y position user	51.036747	flying height	power consumption
shadow margin user	-3.0398193		minimal $P_{tx}$
number of users	1		

Table 3.2: Overview of the configuration.

### 3.2 Increasing traffic with only one drone available

This scenario investigate the same behavior as the previous. Still with one drone but for a higher number of users. The scenario can be divided into two groups. One for a variable flying height but with a fixed number of 224 users which is the number of active users on an average day at 5 p.m. meaning which means it is rush hour resulting in the highest number of simultaneous users for the day[5]. The other scenario has a fixed flying height of 100 m as recommended by [5] but with a variable number of users. To enforce the tool to only use one drone, a facility

capacity is set to one which implies that there is only one spot available in the facility where the UABSs are stored. The tool will still generate as much potential places as there are users in the network. But when the optimization algorithm is done, only one drone will remain.

Parameter	Value	Input variables	Output variables
facility capacity	1	type of antenna flying height number of users optimization strategy	$SAR_{10g}$ power consumption user coverage

Table 3.3: Overview of the configuration.

Four possible configurations are possible because there are two antennae available (equivalent isotropic radiator and a realistic antenna) which can both operate in an power consumption optimized network or an exposure optimized network. These four configurations are investigated for the two groups mentioned above. Both groups can further be divided in four series where The  $SAR_{10g}$ , power consumption and user coverage will be investigated for both groups. The only available drone will be positioned at the fly height of 100 m as recommended in [5]. For the second case, the same output variables are investigated for a varying fly height but with a fixed number of 224 users. Both cases will be investigated for the two types of antennae: the fictional equivalent isotropic radiator and the microstrip patch antenna.

### 3.3 Increasing traffic with an undifend amount of drones

Input variables	Output variables
type of antenna flying height number of users optimization strategy	$SAR_{10g}$ power consumption user coverage

Table 3.4: Overview of the configuration.

When more drones are available, an optimization strategy can be applied. The tool checks the capacity of the base stations and decides thereafter wich base station the user should be connected to. The original algorithm checks all pahts between the user that need to be connected with all drones. Thereafter, the drones which path experience the least path loss and still has the capacity to cover an addition user will be selected. The authors from [9] proposed however annother optimization strategy which tries to minimize electromagnetic exposure and power consumption.

The input variables flying height, transmit power and number of users will be used to see how electromagnetic exposure, power consumption and number of drones are influenced for different optimization strategies and type of antennas.

Since there is no fixed budget limitation, the number of drones are unlimited. The tool will therefore try to connect each user and coverage will be expressed in number of drones required to cover as much users as possible instead of having a limited number of drones as in scenario and therefore has only a limited coverage expressed in percentage.

# 4

## Methodology

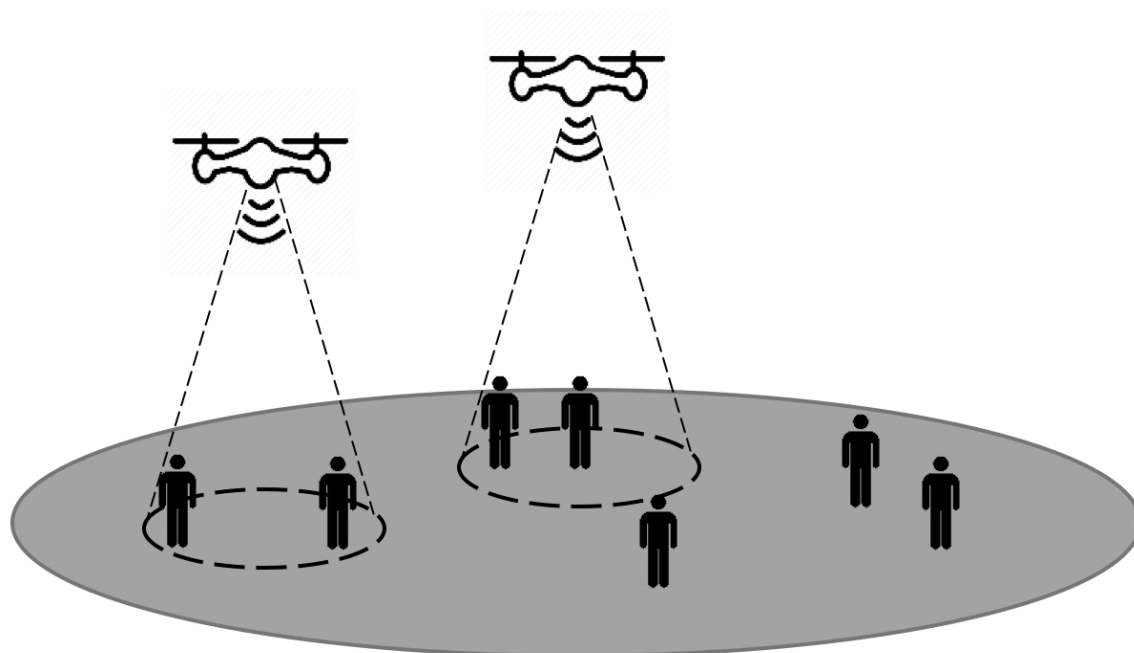


Figure 4.1: Design of the microstrip patch antenna.

## 4.1 Electromagnetic exposure

### 4.1.1 Calculation of the total specific absorption rate

The total whole body SAR ( $SAR_{10g}^{wb}$ ) of a user can be calculated by a simple sum of individual SAR values from the different sources. Formula 4.1 was originally described in [12] for SAR values induced into the head. Using  $SAR_{10g}^{head}$  would however result into incorrect conclusions since the position of the phone relative to the user is unknown. This is because the tool assigns a bitrate to a user depending on the service he is using meaning that users in the network are not only calling but are able of using other services as well like browsing the web. The position of the phone can thus be next to the head but also in front of the user. The induced electromagnetic radiation will therefore be expressed in function of the entire body.

$$SAR_{10g}^{wb,total} = SAR_{10g}^{wb,ul} + SAR_{10g}^{wb,dl} + SAR_{10g}^{wb,neighbours} \quad (4.1)$$

The first parameter,  $SAR_{10g}^{wb,ul}$ , will indicate the absorbed electromagnetic radiation by the whole body originating from the user's own device whereas the second parameter  $SAR_{10g}^{wb,dl}$  will represent the absorbed electromagnetic radiation caused by all the base stations in the considered area. The last factor,  $SAR_{10g}^{wb,neighborhood}$ , specifies the exposure of our user to U/L radiation from other mobile devices. The sections that follow will explain how each value in this formula can be calculated. This can be achieved by first calculating the electromagnetic exposure from each source.

### 4.1.2 Electromagnetic exposure caused by far-field radiation

The electromagnetic exposure to which people are exposed can be categorized in two groups. One of them is near-field radiation which is caused by the user's own device and which will be discussed in 4.1.3. The other type is far-field radiation and will be explained in this section. This kind of radiation is caused by radiators 'far away'. Examples of these types of radiators are UE which belong to other people and UABSs.

#### Electromagnetic radiation from a single source

To determine the total exposure of a single human being or even of the entire network, the electric-field  $\vec{E}$  from a single radiator  $i$  should be calculated. The formula to determine this

electromagnetic value  $E$  (expressed in V/m) for a specific location  $u$  is given in equation 4.2.

$$E_i(u) = 10^{\frac{RRP(u) - 43.15 + 20 \cdot \log(f) - PL(u)}{20}} \quad (4.2)$$

**frequency** The used frequency in the formula above is denoted as  $f$  and is expressed in Mhz. Since LTE is used, this value will be 2600 Mhz.

**Real Radiation Power and EIRP** In formula 4.2, as it was described in [8, 9], RRP was defined as equivalent isotropic radiation power (EIRP). EIRP is the radiation generated by an equivalent isotropic radiator which is a theoretical source of electromagnetic waves that radiate with the same intensity in all directions. The formula to find this EIRP value (in dBm) is described in 4.3 where  $P_t$  stands for the input power of the antenna,  $G_t$  for the gain of the transmitter and  $L_t$  being its feeder loss.

$$EIRP = P_t + G_t - L_t \quad (4.3)$$

This formula, which is constructed out of different gains and losses, misses a factor when accounting for real life radiation patterns. Formula 4.2 solves this by using RRP instead of EIRP which can be defined as follows:

$$RRP(u) = EIRP - attenuation(u) \quad (4.4)$$

The attenuation for a user  $u$  is given based on the angle between the main beam and the user. More details on how this can be implemented is described in 4.3.2. When assuming that  $attenuation(u)$  returns positive values, the attenuation can simply be subtracted from the EIRP-value.

**path loss** At last, formula 4.3 requires the path loss (in dB). In order to calculate this, an appropriate propagation model is required of which several exist. The tool uses the Walfish-Ikegami model because it performs well for femtocell networks in urban areas [5]. The chosen propagation model consists of two formulas depending on whether a free line of sight (LOS) between the user and the base station exists or not. Both formulas expect a distance in kilometre.

### Combining exposure

The electromagnetic exposure for a given location originating from different sources can be calculated with formula 4.5 (in V/m).  $E_i$  stands for the electromagnetic exposure from source  $i$  and  $n$  stands for all far-field radiators of a certain category which will either be UABSs or UE

from other people.  $E_{tot}$  was originally calculated for each  $x$  meters [9]. In the tool, the exact location of the users is known and  $E_{tot}$  will thus only be calculated for locations where a user is positioned.

$$E_{tot} = \sqrt{\sum_{i=1}^n E_i^2} \quad (4.5)$$

### Converting far-field electromagnetic exposure to $SAR_{10g}^{wb}$

Formula 4.1 expects that the electromagnetic radiation is expressed into  $SAR_{10g}^{wb,dl}$  and  $SAR_{10g}^{wb,neighbours}$ . The calculation for both values is in fact identical. The only difference is the sources where the first one is for UABSs and the second one for UE. Physically seen, they are both whole body SAR values induced by far-field radiation ( $SAR_{10g}^{ff,wb}$ ).

The electromagnetic radiation needs to be converted into  $SAR_{10g}^{ff,wb}$ . This conversion factor is based on Duke from the Virtual Family. Duke is a 34-year old male with a weight of 72 kg, a height of 1.74 m and body mass index of 23.1 kg/m [13]. Research shows that the conversion factor for WiFi is  $0.0028 \frac{W/kg}{W/m^2}$ . Since WiFi, at a frequency of 2400 Mhz, is very close to LTE, at 2600 Mhz, it is assumed in [13] that this value is also applicable for LTE. This constant converts the power flux density  $S$  (with units  $\frac{W}{m^2}$ ) to the required  $SAR_{10g}^{ff,wb}$ . To make this possible, the electromagnetic radiation from formula 4.5 (expressed in  $V/m$ ) should first be converted to the power flux density which formula 4.6 before formula 4.7 can be applied.

$$S = \frac{E^2}{337} \quad (4.6)$$

$$SAR_{10g}^{wb,ff} = S * 0.0028 \quad (4.7)$$

### 4.1.3 Electromagnetic exposure caused by near-field radiation

When a user is operating his device, a part of the U/L radiation will enter his body despite the fact that the traffic is destined for the serving UABS. So the electromagnetic exposure won't be limited by D/L traffic from UABSs or U/L traffic from other UE but also from U/L traffic from his own device.

### Localized Specific Absorption Rate

When assuming that all users hold their device next to their ear, a localized SAR-value for the head  $SAR_{10g}^{head}$  can be calculated. International Electrotechnical Commission (IEC) defines in IEC:62209-2 a maximum for a 10g tissue  $SAR_{10g}^{head}$  as 2 W/kg and a maximum for a 1g tissue  $SAR_{1g}^{head}$  as 1.6 W/kg. Most countries, including Belgium, enforce the 10g model and will, therefore, be the point of reference for this master dissertation. The  $SAR_{10g}^{head}$  values are phone dependent. The values reported by mobile manufactures are worst-case scenarios meaning that the values are measured when the phone is transmitting at maximum power. This is an understandable decision but won't result in a realistic scenario since modern cellular networks use power control mechanisms to prevent over radiation of a nearby device. UE will therefore never use more energy than necessary to maintain a connection. To compensate for this overestimation, the actual  $SAR_{10g}^{head}$  of each user will be predicted. These will, however, remain an estimation since the position of the phone relative to the head differs from user to user. For example, by holding the phone differently, a hand can absorb more or less electromagnetic radiation. The SAR values will also depend on the age of the user, especially children who experience on average higher exposure in the brain regions because of different anatomical proportions [10, 18].

$$SAR_{10g} = \frac{P_{tx}}{P_{tx}^{max}} * SAR_{10g}^{max} \quad (4.8)$$

Equation 4.8 will be used to predict the actual  $SAR_{10g}^{head}$  of a certain user with  $P_{Tx}^{max}$  being the maximum transmission power for a phone which is in LTE and UMTS 23 dBm [19, 10]. The actual transmitted power ( $P_{tx}$ ) is calculated with equation 4.9 where  $P_{sens}$  stands for the receiver sensitivity and  $PL$  the path loss between sender and receiver.

$$P_{tx} = P_{sens} + PL \quad (4.9)$$

The  $SAR_{10g}^{max}$  value is different for each mobile device. An average is calculated based on 3516 different phones from various brands using a German database [20] for which an overview can be found in fig. 4.2. When the phone is positioned at the ear, an average of 0.7 W/kg is found with a standard deviation of 0.25 W/kg which are very similar results as in ref. [21]. The median of 0.67 is used.

### Whole body specific absorption rate

The position of the phone relative to the user's body is however unknown. The tool assigns different bitrates to different phones implying that some users are calling and therefore probably holding their phone next to their ear while another part is using other services like browsing the web. For this reason expects formula 4.1 that the specific absorption rate is expressed for



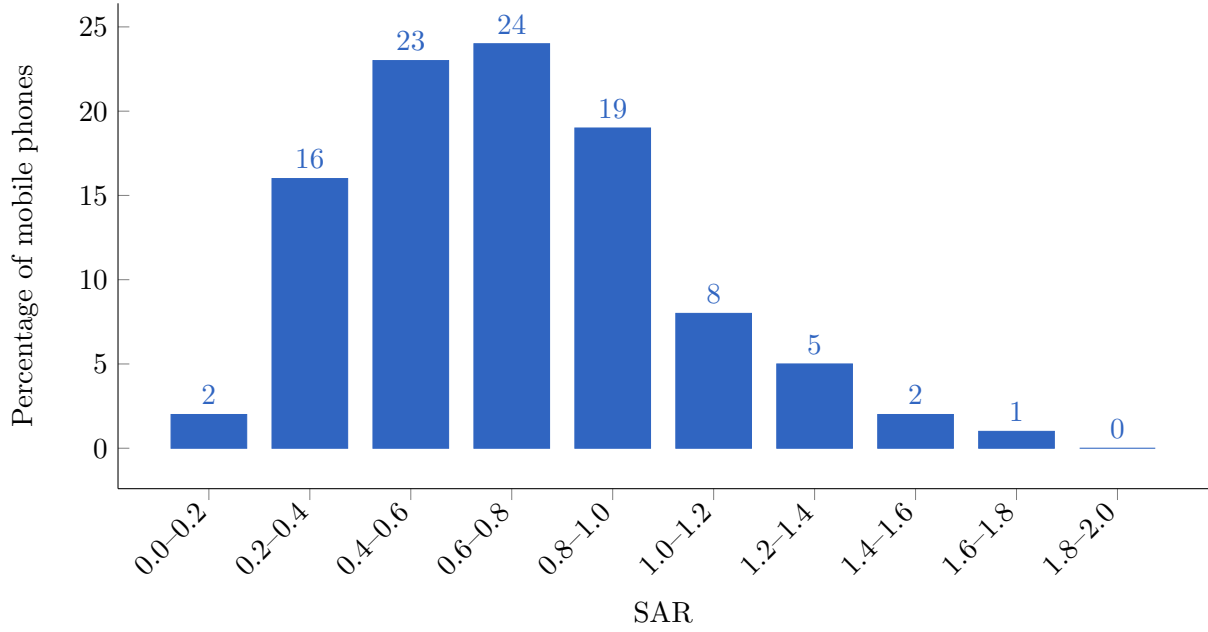


Figure 4.2: Distribution of how many phones belong to a certain SAR interval. Upper boundary not included

the entire body instead of localized  $SAR_{10g}^{head}$ . The conversion factors for Duke from the Virtual Family will be used again as which was already the case in 4.1.2. The constant to convert U/L exposure to  $SAR_{10g}^{wb,ul}$  for WiFi is defined to be  $0.0070 \left( \frac{W/kg}{W} \right)$  [13] which leads to eq. 4.10.

$$SAR_{10g}^{wb,ul} \left( \frac{W}{kg} \right) = 0.0070 \left( \frac{W/kg}{W} \right) * P_{tx}(W) \quad (4.10)$$

#### 4.1.4 Defining an antenna

A microstrip patch antenna is chosen because it allows easy production but more important, it has a low weight and has a thin profile causing it to be very aerodynamic which is useful when attaching it to a drone [16].

The dimensions of the antenna depend on the frequency it is operating and the characteristics of the used substrate. The antenna will be radiating at a center frequency  $f_0$  of 2.6 Ghz. Each substrate has a dielectric constant  $\epsilon_r$  representing the permittivity of the substrate and depends on the used material. Substrates with a high dielectric constant and low height reduce the dimensions of the antenna while a lower dielectric constant with a high height improves antenna performance. In this paper, a substrate like glass is chosen because of the higher dielectric constant of  $\epsilon_r = 4.4$  compared to materials like teflon with only a dielectric constant of  $\epsilon_r = 2.2$  [15]. Doing this in combination with an antenna height of 2.87 mm will decrease the dimensions

of the entire antenna surface which comes in handy for the limited space on drones.

description	symbol	value
center frequency	$f_0$	2600 Hz
dielectric constant	$\epsilon_r$	4.4
height of the substrate	$h$	0.00287 m

Table 4.1: Overview of configuration parameters

The dimensions of the radiating patch can be calculated with the formulas from [15] and [17] using the defined values from table 4.1. In that way, the width  $W$  is calculated using formula 4.11.

$$W = \frac{C}{2 * f_0 * \sqrt{\frac{\epsilon_r + 1}{2}}} \quad (4.11)$$

With  $C$  being the speed of light,  $f_0$  the center frequency of 2600 MHz and a dielectric constant  $\epsilon_r$  of 4.4. This results in a width of 3.51 mm.

In order to find the length of the radiating patch, some other values need to be determined first. Formula 4.12 will calculate the effective dielectric constant ( $\epsilon_{eff}$ ).

$$\epsilon_{eff} = \frac{\epsilon_r + 1}{2} + \frac{\epsilon_r - 1}{2} * \left(1 + 12 * \frac{h}{W}\right)^{-\frac{1}{2}} \quad (4.12)$$

This formula requires the width found in the previous formula along with the dielectric constant and substrate height from table 4.1. This will result in a  $\epsilon_{eff}$  of 3.91.

$$L_{eff} = \frac{c}{2 * f * \sqrt{\epsilon_{eff}}} \quad (4.13)$$

Now formula 4.13 can be used to calculate effective length ( $L_{eff}$ ) which results in 29.16 mm.

$$\Delta L = 0.412 * h * \frac{(\epsilon_{eff} + 0.3) \left(\frac{W}{h} + 0.264\right)}{(\epsilon_{eff} - 0.258) \left(\frac{W}{h} + 0.8\right)} \quad (4.14)$$

Eventually, the length extension is found with formula 4.14 by substituting the values from above. Doing so determines that the  $\Delta L$  equals 1.3071 mm.

Finally, the length of the patch can be calculated using the expression:  $L = L_{eff} - 2 * \Delta L$  which results in 26.55 mm.

The dimensions of the radiation patch are now known. The only remaining questions are the dimensions of the ground plane and dielectric substrate to which the radiation patch is attached.

The transmission line model is in fact only applicable for an infinite ground plane but it has been proven that similar results can be achieved if the ground plane's dimensions are bigger than the patch by approximately 6 times the height of the dielectric substrate [15, 17].

$$L_g = 6 * h + L \quad (4.15)$$

$$W_g = 6 * h + W \quad (4.16)$$

Therefore, should the length of the ground plane  $L_g$  be at least 0.0438 m and a width  $W_g$  at least 0.0524 m. A schematic overview of how the antenna will look like is given in figure 4.3.

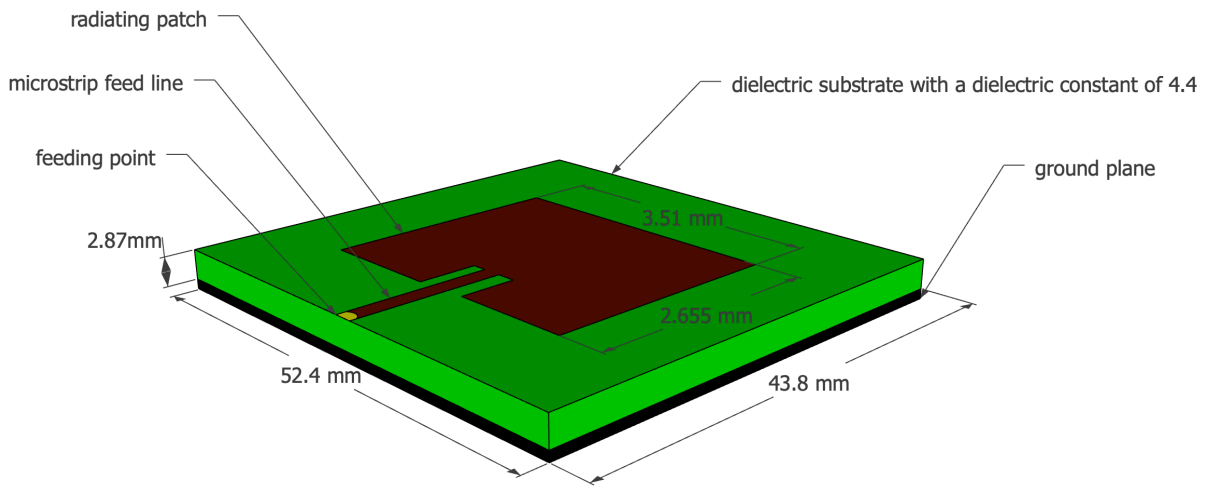


Figure 4.3: Design of the microstrip patch antenna.

#### 4.1.5 Radiation pattern

Mathlab is able to generate the radiation pattern for this microstrip patch antenna. The code in listing 1 starts with defining the dielectric substrate which will be glass with a dielectric constant of 4.4 and a height of 0.00287 m. Thereafter, the microstrip patch antenna is generated with the `width` and `length` being the dimensions of the radiation patch and the `GroundPlaneLength` and `GroundPlaneWidth` the dimensions of the ground plane and dielectric substrate. The `FeedOffset` is the relative offset from the center where the radio frequency power is fed to the radiating patch which will here be at the edge. This is in figure 4.3 indicated with the yellow dot. At last, the `dielectric-object` is substituted into the `patchMicrostripInsetfed-object`.

Generating the pattern is done with the `pattern`-command. The first value is the `patchMicrostripInsetfed` object followed by the frequency in which the antenna will be op-

erating. Optionally, an azimuth value can be parsed like in line 7 and 8 where 90 and 0 stand for relatively the H-plane and E-plane.

```

1  d = dielectric("Name",'glass',"Thickness",0.00287,"EpsilonR",4.4)
2  p = patchMicrostripInsetfed("Width",0.0351,"Length",0.02655,
3      "GroundPlaneLength",0.0438,"GroundPlaneWidth",0.0524,
4      "FeedOffset",[-0.021885 0],"Substrate", d)
5
6  pattern(p,2.6e9, "CoordinateSystem", 'polar', "Normalize",true)
7  pattern(p,2.6e9, 90, "CoordinateSystem", 'polar', "Normalize",true)
8  pattern(p,2.6e9, 0, "CoordinateSystem", 'polar', "Normalize",true)

```

Listing 1: Matlab code to generate radiation pattern for a microstrip patch antenna

Running the configuration from listing 1 will generate the radiation pattern from figure 4.4. When running the same configuration for a slightly bigger square ground plane with an edge of 0.060 m, the radiation pattern from 4.5 is achieved. Both radiation patterns show an aperture angle of approximately  $90^\circ$ . It becomes clear that the radiation pattern from figure 4.4 has a higher attenuation in the direction it is not facing compared to the radiation pattern of figure 4.5. If it is assumed that drones fly lower than some users are positioned in some buildings, the pattern of 4.5 would be a better approach. However, for the continuation in this master dissertation, the radiation pattern from figure 4.4 is assumed since the antenna is the smallest and therefore more suitable to attach to the limited space available under a drone. A data sheet of the exact values from both radiation patterns can be found in appendix A.

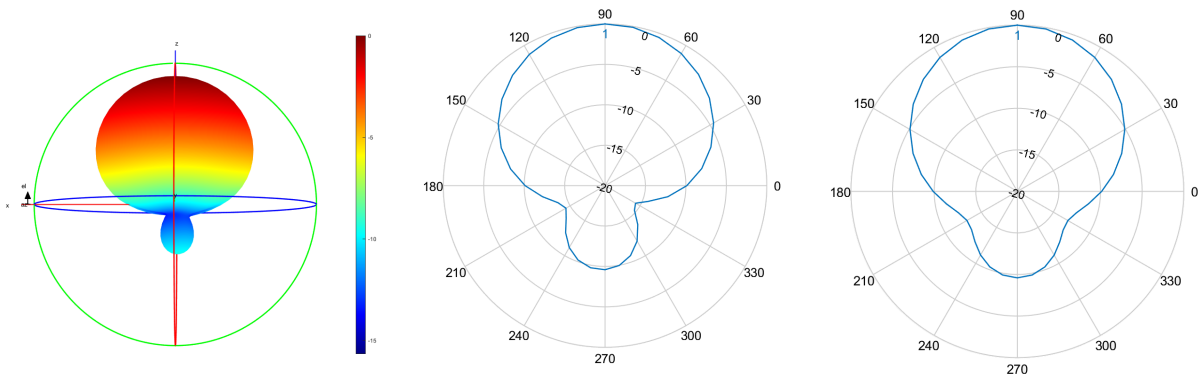


Figure 4.4: Radiation pattern 1: 3D model of the entire pattern on the left with the configuration as described above. In the middle a 2D radiation pattern of the E-plane and at the right a 2D model of the H-plane.

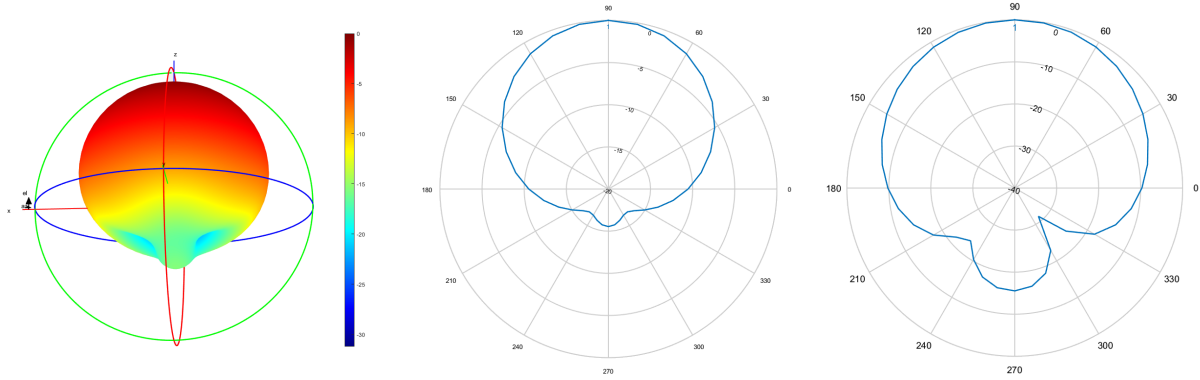


Figure 4.5: Radiation pattern 2: Generated with a groundplane of 0.06m by 0.06m. On the left is the 3D model of the entire pattern plotted. In the middle a 2D radiation pattern of the E-plane and at the right a 2D model of the H-plane.

## 4.2 Optimizing the network

The network, as originally defined in the deployment tool, tried to minimize power consumption by connecting the user to a base station which experienced the lowest path loss. A second optimization strategy is introduced, based on the fitness function described in [9].

$$f = w * \left(1 - \frac{E_m}{E_{max}}\right) + (1 - w) * \left(1 - \frac{P}{P_{max}}\right) * 100 \quad (4.17)$$

Formula 4.17 returns a fitness value. Users are connected to different UABSs and each time the fitness value is calculated. The user will eventually be connected to the drone which resulted in the highest fitness value. This process is repeated for each user.  $w$  is the importance factor of electromagnetic exposure ranging from 0 to 1, boundaries included. A  $w$  set to zero means that electromagnetic exposure is not important. Such a network will therefore be called a power consumption optimized network. Likewise, a  $w$  set to one means that minimizing exposure is top priority and will result in an exposure optimized network.  $P_{max}$  is the power consumption of all UABSs, both active and inactive, when radiating at the highest possible level while  $P$  is the effective used power by the current designed network. This will be the power required for the flying drones themselves and their antenna.  $E_m$  will be the weighted exposure of the average user for the current designed network and  $E_{max}$  the electromagnetic exposure when all antennae are at their highest power level.

When optimizing the network, it is not only important to consider the average exposure of all users, but also to limit high extremes [9]. A weighted average will be used not only considering the median but also the 95 percentile from all users their D/L exposure using formula 4.18. Since both values are considered to have equal importance, the weight factors  $w_1$  and  $w_2$  will

both have an equal importance of 50%.

$$E_m = \frac{w_1 * E_{50} + w_2 * E_{95}}{w_1 + w_2} \quad (4.18)$$

## 4.3 Implementation

### 4.3.1 Network planning, bringing it all together

The existing algorithm as described section 2.1 is extended to support different optimization strategies by using the formulas from section 4.2. As explained in State of the Art, the program starts with the preparation of the network by distributing the users over the network and assigns a bitrate that each user will require. Thereafter, the tool tries to solve this network by assigning a UABS above each user. This master dissertation will only cover fixed flying heights meaning that a certain position is only infeasible if it is obstructed by a building.

Solving the network is done by calculating the path loss between all users and between users and UABSs. Thereafter, the tool iterates over each user and tries to connect that user to each UABS. This connection is not always possible. A UABS might be saturated with users and won't be able to cover yet another user or maybe the user is so far away that in order to cover that user, the UABS would exceed its maximum allowed input power. If however a connection is possible, the user will be connected to that UABS and the fitness function from section 4.2 is calculated. Only the connection which results in the best fitness value for the entire network will be used. Thereafter, the tool shifts to the next user.

Up till now, the tool assumed an unlimited number of drones but this is an unrealistic scenario. Certainly when high number of users are present in the network. The number of available drones can be limited by defining the capacity of the facility where the drones are stored. If such a capacity is defined and the number of active drones exceed this limitation, the tool will delete the necessary drones starting by those who cover the least number of users. These users will now become uncovered.

### 4.3.2 Implementation of the radiation pattern

The deployment tool originally only supported equivalent isotropic radiator's. The tool has thus been extended and is fully configurable allowing any possible antenna in any possible orientation with the usage of a XML-file. The configuration described in this file will apply to all UABSs.

The orientation is done using two values called ‘downtilt’ and ‘north offset’. The first value defines the downtilt angle under which the antenna is pointing. A downtilt angle of zero degrees is perfectly horizontal and an antenna with a downtilt angle of  $90^\circ$  will be pointing straight to the ground. This parameter only supports positive values ranging from  $0^\circ$  to  $360^\circ$  (upper boundary not included). An antenna pointing to the sky would therefore require a value of  $270^\circ$ . The second value, the north offset, defines the azimuth orientation of the drone. The value given to this parameter indicates the offset between the north and the horizontal direction to which the antenna should be pointing to. The value once again ranges from  $0^\circ$  to  $360^\circ$  with the upper boundary not included. The angle is calculated in counter clock wise orientation. For instance, a north offset of  $270^\circ$  will let the UABS point to the east.

Thereafter, the normalized radiation pattern is supplied to the tool. The actual pattern is three dimensional. To simplify this, slices perpendicular to the az-axis are extracted. These are indicated at figure 4.6 with azimuth cuts. With an angle of  $90^\circ$  four slices are achieved, each consisting out of elevation cuts. The intersection of an elevation and azimuth plane corresponds with a certain attenuation which is fed to the tool. Figure 4.6 shows only 3 elevation planes. The radiation pattern used in the tool has an attenuation every  $10^\circ$ . In other words, a slice consists of 19 values ranging from  $0^\circ$  to  $180^\circ$  (boundaries included).

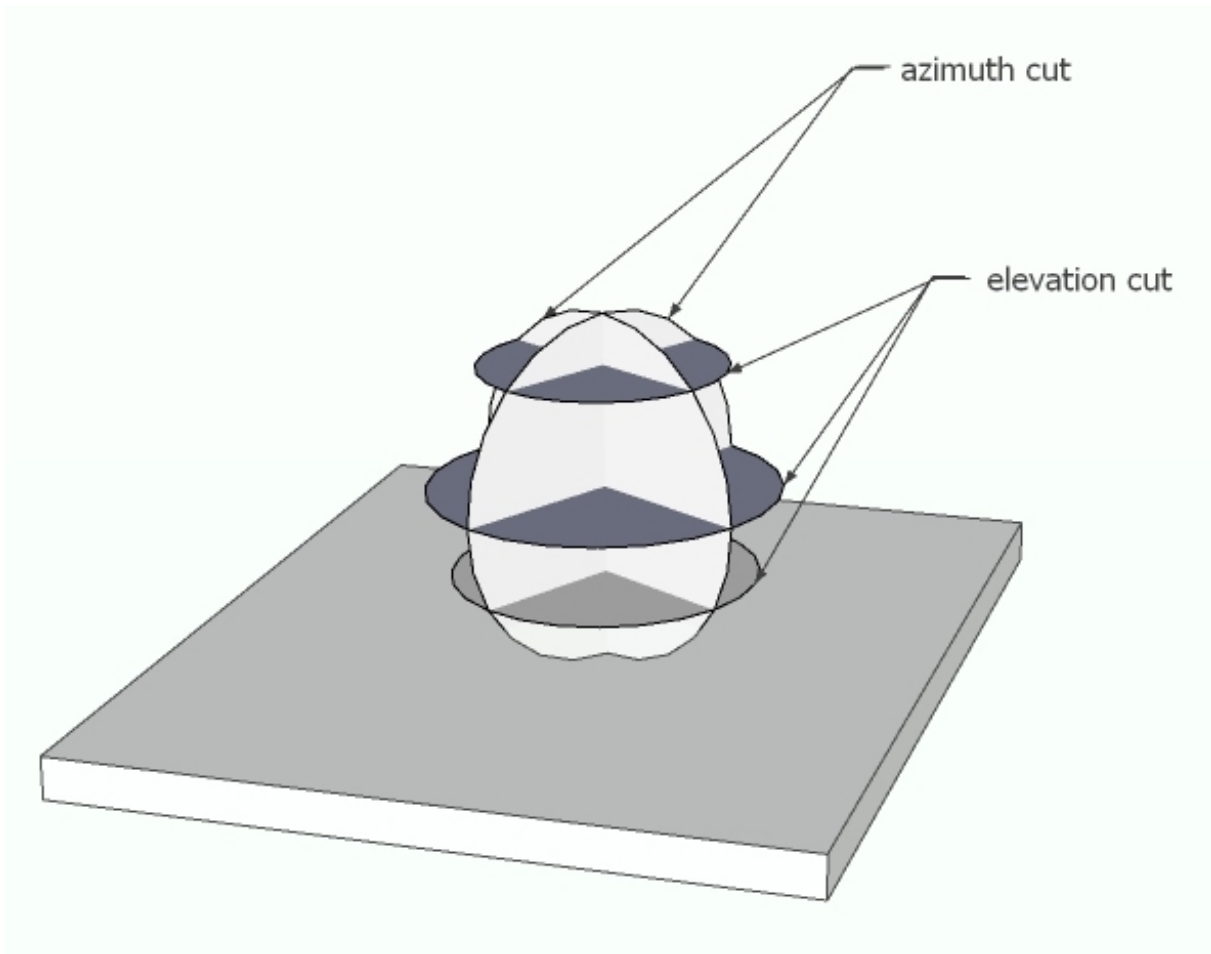


Figure 4.6: Schematic example of slices in a radiation pattern.

The number of required slices depends on the complexity of the radiation pattern. For symmetrical radiation patterns, like in figure 4.4 and 4.5, two azimuth cuts perpendicular to each other dividing the radiation pattern in 4 azimuth-slices are definitely sufficient. However, this might not be the case for radiation patterns with a more complex structure containing several side lobes. To tackle this issue, more azimuth-slices can be defined for increased precision. Each slice should however contain an equal amount of elevation slices. A concrete example of a configuration file can be found in appendix B.

When the attenuation of a user from a certain UABS needs to be known, the elevation and azimuth angles between the user and the antenna's direction should be calculated. Figure 4.7 represents a radiation pattern with the black dot indicating the user for which the attenuation needs to be calculated. The small black lines represent azimuth and elevation planes. The tool knows the exact attenuation only at the intersection of those lines. The chance that a user is positioned at such an intersection is very small. Therefore, the attenuation for the requested



point has to be estimated using bilinear interpolation. First, the attenuation is estimated at the intersection of the red and orange line using linear interpolation on the horizontal axis with the known values at the end of the red line. The same is done for the orange-green intersection using the known values at the end of the green line. Finally, linear interpolation is applied to the y-axis for the black dot on the orange line using the estimated values at the end of the orange line.

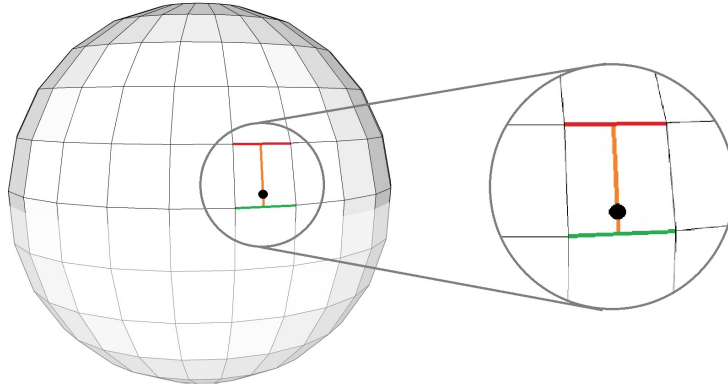


Figure 4.7: Schematic example of how bilinear interpolation works.

### 4.3.3 Performance improvement

#### Calculating path loss

The path loss is required for several formulas. For instance, each user decides whether a UABS is feasible based on the path loss but also the calculations for the downlink electromagnetic exposure require this value to be known. The formulas for the whole body  $SAR_{10g}$  require not only the path loss between the user and all UABSs but even the path loss between users themselves. These path loss calculations are based on the Walfish-Ikegami model that causes a high computational load. The calculation between two points stands completely free from any other calculation between any other point and is therefore a suitable candidate to be multithreaded. The deployment tool creates two thread pools. The first pool creates a thread for each user where each thread calculates the path loss between the user assigned to him and all possible UABSs, causing a time complexity of  $n^2$ . Each user stores all path losses between himself and any other UABS and result therefore in a total space complexity of  $n^2$ . When all users are finished, the thread pool is shut down and the second one is created for the same calculations but between users. The pool will, just like the previous, create threads for each user but has an important difference. When a certain user calculates the path loss to another user, this path loss also applies for the other direction. The tool saves time by calculating the path loss only once and stores the path loss at both users. It is therefore sufficient that a given user only

calculates path losses of users at his right side, since the other path losses will be calculated by the users on his left. This results in a time complexity of only  $n(\frac{n}{2})$ . When the last user finishes his thread, all users know the path loss of all other users causing a space complexity of  $n(n-1)$ .

### Limiting antenna searching

The user needs to be connected to the ‘best’ base station. To identify this best UABS, the user should be connected to each base station and the fitness value 4.17 of the network has to be evaluated. The connection that resulted in the best fitness function will be added to the solution. This process is repeated for each user but can further be improved. A user will like to be connected to either the UABS directly above him or to a UABS in the direct neighbourhood. Time complexity can thus be improved by not considering drones outside a certain radius. An ideal data structure for neighbourhood-search is a KD-tree. This data structure is based on a binary tree and is optimal for objects with multiple keys. Objects are thus positioned in K dimensions where each node splits the hyperplane over exact one dimension. The dimension that needs to be split depends on the level of the KD-tree where that node is situated. In this case, the x and y coordinate will be used in a 2D-tree (k=2) like in figure 4.8.

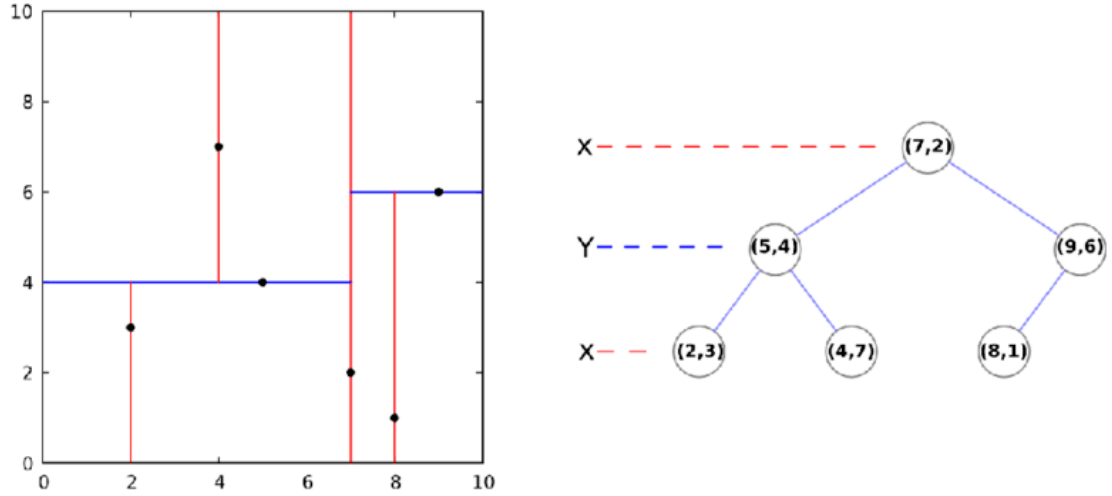


Figure 4.8: Example of a KD-tree in two dimensions

In this case the choice was made to only consider UABSs within a radius of half a kilometer. This will result in 23 UABSs on average when applied to a default scenario of 224 UABSs at a flying altitude of 100 m.

# 5

## Results and discussion

### 5.1 Scenario 1: one user and one base station

The network contains only one user for this scenario. This means that there is only one location possible for the drone which is just above the user. This section will investigate minimal required transmission power and SAR values from different sources. **power consumption te doen**

#### 5.1.1 The influence from the maximum transmission power

LTE makes usages of power control meaning that no more power will be used then strictly necessary. The actual transmit power  $P_{tx}$  therefore ranges between 0 and the maximum input power.  $P_{tx}$  is zero when the UABS doesn't cover anybody. Increasing the maximum transmission power won't influence the power consumption or  $SAR_{10g}$  because the UABS won't use more then strictly required. It is therefore more useful to match the actual transmission power against a variable flying height. Figure 5.1 shows a logarithmic relationship showing that  $P_{tx}$  increases fast at low altitude but slows down at higher altitudes.

Figure 5.1 shows the minimal required energy by an equivalent isotropic radiator in order to reach the user just below him. As already discussed in 3.1, the user is outdoor and just below the

UABS. There is thus a free line-of-sight between both radiators. It is clear from figure 5.1 that a step function is achieved because multiple flying heights correspond to the same transmission power. When the flying height increases, so does the path loss. LTE tries to counteract this by increasing the power level. Each time the path loss becomes too high, the power level of the antenna increases with one dBm. Doing so, decreases path loss allowing the antenna to reach the user again.

After a jump in the step function, there is an overestimation meaning the input power increased more than necessary. So multiple flying heights correspond with the same  $P_{tx}$ . dBm has a logarithmic scale meaning that while 10 dBm equals 10 mW, 20 dBm equals 100 mW. This explains why the black lines become longer at higher flying altitudes. Each time the power level increases with one dBm, the overestimation becomes larger.

If the tool would make usage of smaller step size, a more continuous logarithmic function would be achieved. This would however worsen the time complexity because increasing the power level to exceed the path loss would happen in much smaller steps. The red line indicates the default maximum transmission power used during simulations. In a free line-of-sight scenario with only one user, a UABS can fly up to 387 meters before losing connection.

This scenario is investigated with a microstrip patch antenna using power consumption optimization and however an equivalent isotropic radiator doesn't have any attenuation while a microstrip patch antenna does, these parameters does not matter. This is because the user is positioned in the perfect center of the main beam where there is no attenuation in either cases. Also the optimization won't make a difference. The goal of the strategy is to decide which drone is most suitable for which users. Since there is only one user and one possible position for the drone, both optimization strategies behave identical.

### 5.1.2 Influence of the flying height

This section investigates how the flying height of a UABS influence  $SAR_{10g}$  and power consumption. In figure 5.2 becomes clear that with an increasing flying height, the specific absorption rate grows exponentially which is also the case for the power consumption in figure ??.

Figure 5.2 shows represents the induced electromagnetic radiation for our user and shows that for low flying drones, UABSs are the main source of electromagnetic radiation which is indicated with the green line. This changes around 80 meters where U/L electromagnetic radiation of the UE (indicated with the red line) exceeds D/L radiation in order to still be able to reach the high flying UABSs.

The green line (representing the  $SAR_{10g}^{basestation}$ ) shows the same discontinuous behaviour from in

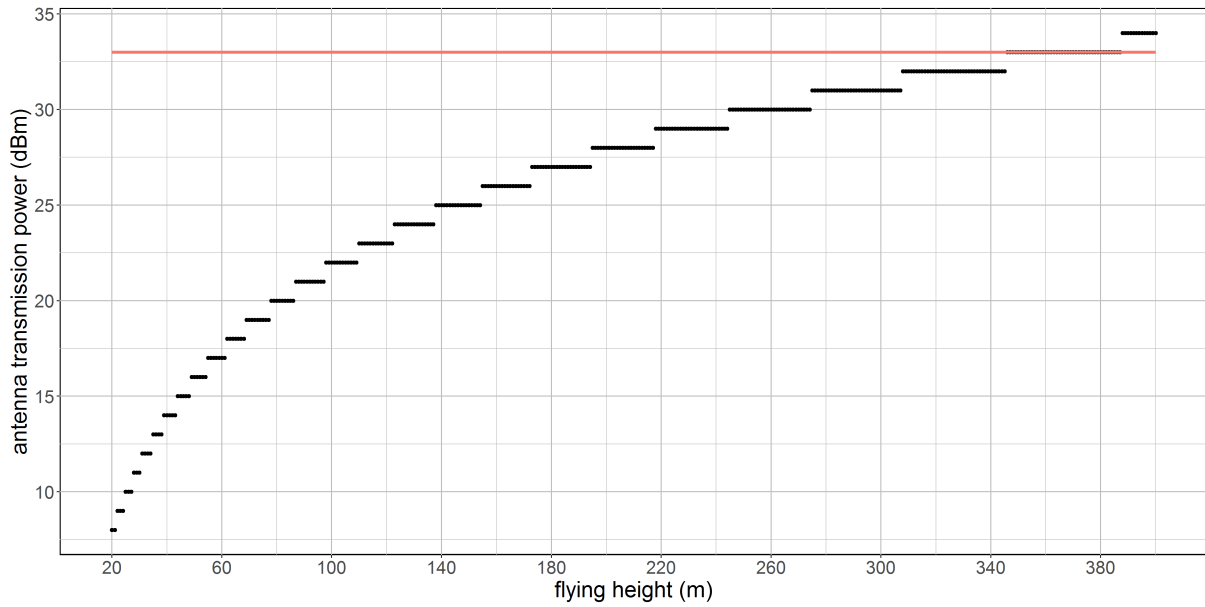


Figure 5.1: Minimal required transmission power by the antenna to reach the ground just below him. The red line shows the default maximum transmission power.

figure 5.1. As explained before, LTE makes usage of power control. Meaning that the power transmission only increases when path loss increases up to the point where the power level exceeds its maximum after which connection is lost completely and exposure drops to zero. This behaviour causes the electromagnetic radiation experienced by the user to be almost constant. The slightly visible variation in the green line has the same reason as why figure 5.1 shows a step function. The green line can be simplified to a constant linear line. This means that the electromagnetic radiation before it was converted into UABS using the formulas from section 4.1.2 was also constant because of power control. The exposure is in other words a constant fraction of power and distance like shown in equation 5.1.

$$\vec{E}(V/m) = \frac{\Delta U(V)}{\Delta x(m)} \quad (5.1)$$

Figure 5.2 doesn't show radiation from neighbours, because there are none present in this scenario. Finally, all these values are added as explained in formula 4.1 and indicated with the blue line.

power consumption to do

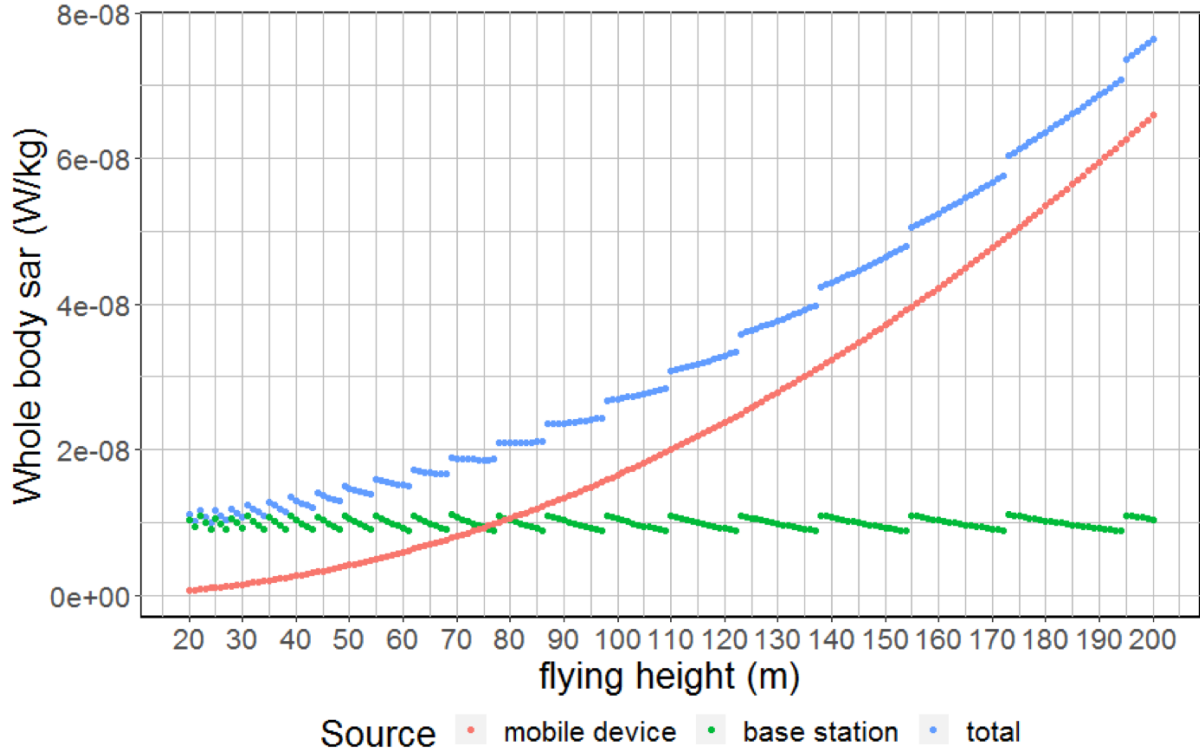


Figure 5.2: How SAR values from different sources are influenced by different flying altitudes

## 5.2 Scenario 2: increased traffic

This scenario has just like the previous scenario only one drone. However, more users will be present in the network. First, a variable flying altitude is investigated for a fixed number of 224 users. Secondly, the flying height is set to 100 metres with a variable number of users. When designing the network, there will be as much possible drone locations as there are users in the network and the tool will consider all of them. It's only when the programme is finished, that one drone remains.

### 5.2.1 Influence of the flying altitude

This scenario investigates how the network consisting of one UABS behaves when applied on an ordinary day during rush hour. On average, 224 active users are distributed uniformly over the city center of Ghent. Chart 5.3 shows how the downlink exposure is clearly influenced by the flying height of the UABS. This is because if a drone flies higher, there is less penetration loss from obstructing buildings.

A power consumption optimized network with an EIRP antenna (green) has the highest expo-

sure. This is logical when comparing with an EIRP antenna in an exposure optimized network (red). However, when looking at chart 5.6, the power consumption in a power consumption optimized network is worse than in an exposure optimized network. To understand this, the behavior of the deployment tool needs to be understood first. A power consumption optimized network will result in few high powered UABSs because increasing the input power of an antenna cost less then activating a new drone. Likewise, an exposure optimized network generates a lot of low powered UABSs because the lower the antenna's power, the lower the exposure. This has the consequence that the cover radius is less and therefore requiring more drones and powering up more drones cost more energy. When only limited amount of UABSs are available, like only one in this scenario, the tool will only keep UABSs which cover most of the users. Therefore, is the power consumption in a power consumption optimized network way higher.

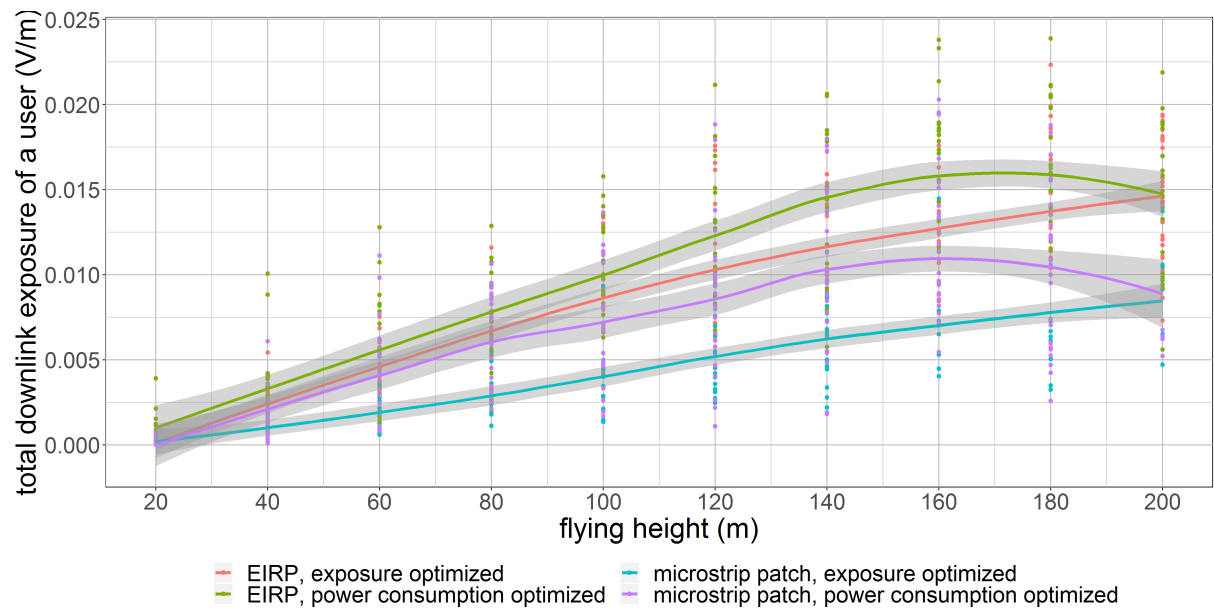


Figure 5.3: The influence of the flying height on the weighted average downlink exposure of users in the network.

The correctness of figure 5.3 is proven with figure 5.4 by investigating the scenario with only two users. The two users who will be referred to by ‘red’ and ‘blue’ user are 90 metres separated from each other with a building between them. Scenario 1 already explained that the charts can be simplified and the blue line from fig. 5.4 remains in fact constant between the zero and 130 metres. The chart shows that the UABS is positioned above the blue user. The orange user is in non line of sight (NLOS) as long as the UABS remains below 20 metres.

Once the UABS increases its flying altitude, the orange user becomes into LOS but still remains uncovered. This is because the tool initially locates a possible UABS above each user and thereafter performs a fitness function. The applied fitness function must have decided that it is better to connect each user to the UABS above him. At a final state, the tool checks whether the number of online drones does not exceed the capacity of the facility which is here the case. The tool therefore deactivates one UABS causing the orange user to be uncovered. One could

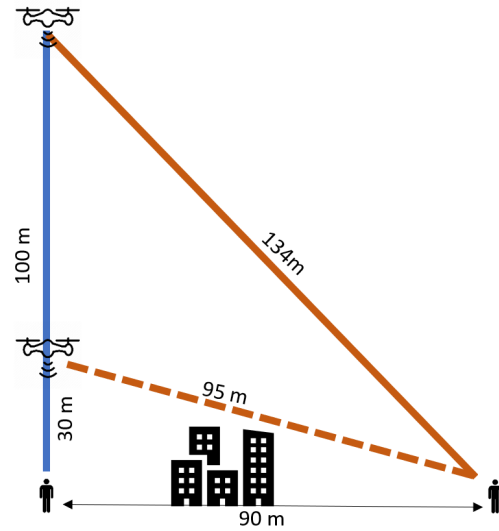


Figure 5.5: Schematic overview of scenario 2 with only 2 users.

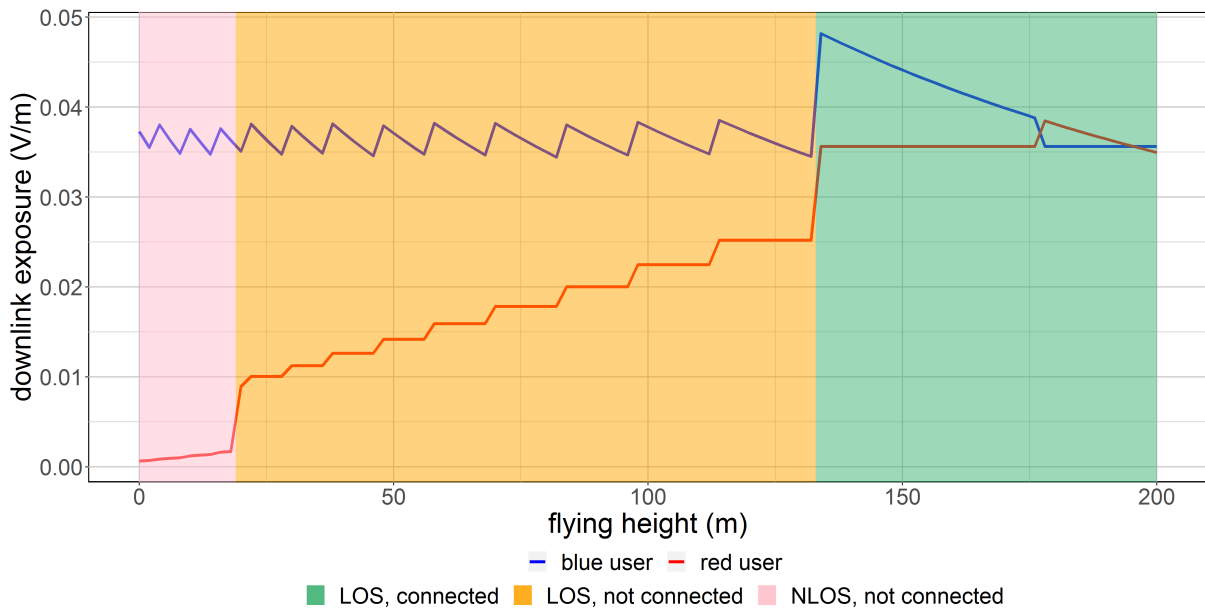


Figure 5.4: Scenario 2 with only 2 users. The coloured areas are only applicable for the orange user. The blue user is connected during the entire time.



argue that the the orange user should be connected to the online drone who is only 90 metres away. This would however require the online drone to increase his power consumption which would make the decisions made by the optimization strategy obsolete.

When the drone flies higher, the difference in distance between both users and the base station decreases. In other words, the Pythagorean theorem shows that when the flying height of the UABS increases, the distance with the blue user increases faster compared to the distance between that same UABS and the orange user. This is also illustrated in figure 5.5.

At 130 metres, the tool decides to connect both users to the same UABS. Therefore, it increases it's power consumption so the orange user would have the minimal required electromagnetic exposure. This has of course a negative influence for the blue user who is way closer and experience now a much higher exposure level.

Around 180 metres, the orange and blue line switch. This is because the drone switches position. As explained before, the tool assigns two possible drones, one above each user. The tool must have decided that connecting both users to the other drones improves the fitness function of the entire network even though that difference might be very little.

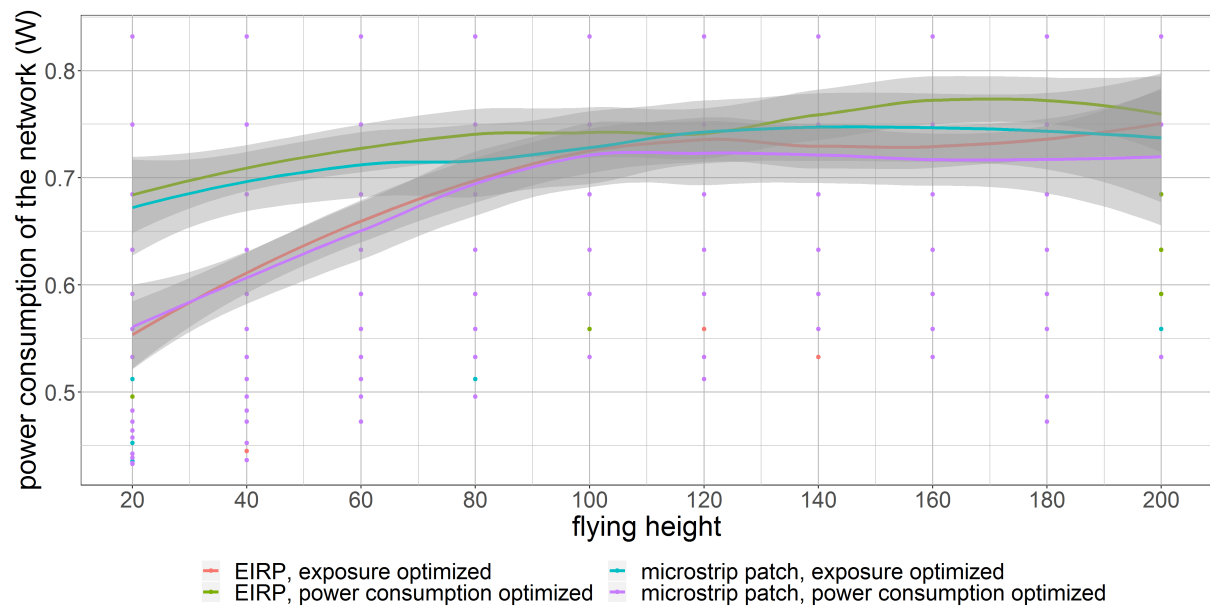


Figure 5.6: The influence of the flying height on the total power consumption of the network.

Uitleg over deze grafiek

Chart 5.7 shows that the flying height has a positive influence on the user coverage. When a UABS flies higher, there is less path loss between the user and the drone caused by buildings but also the path loss to neighbouring users decreases as explained with figure 5.4 and 5.5. Also the increasing D/L exposure from figure 5.3 confirms the that the user coverage should grow.

As mentioned before, a power consumption optimized network will result in few high powered UABSs. The tool removes all UABSs except the one with most users. The network therefore exist out of one high powered UABS compared to the exposure optimized network with one drone which will be less powered. Since green has a higher power level, also more users will be covered.

When replacing the fictional EIRP antenna with a microstrip patch antenna, the percentage of covered users drops for both optimization strategies. This is because users who have a higher horizontal distance between themselves and the UABS, experience a higher attenuation. Also, when a microstrip patch antenna is positioned higher, the range of the antenna increases since the angle between the user and the UABSs main lob decreases. The user will therefore experience less attenuation.

It becomes also clear that this advantage is limited. For a scenario of 224 users and one drone, the user coverage won't increase significantly any more around an altitude of 120m.

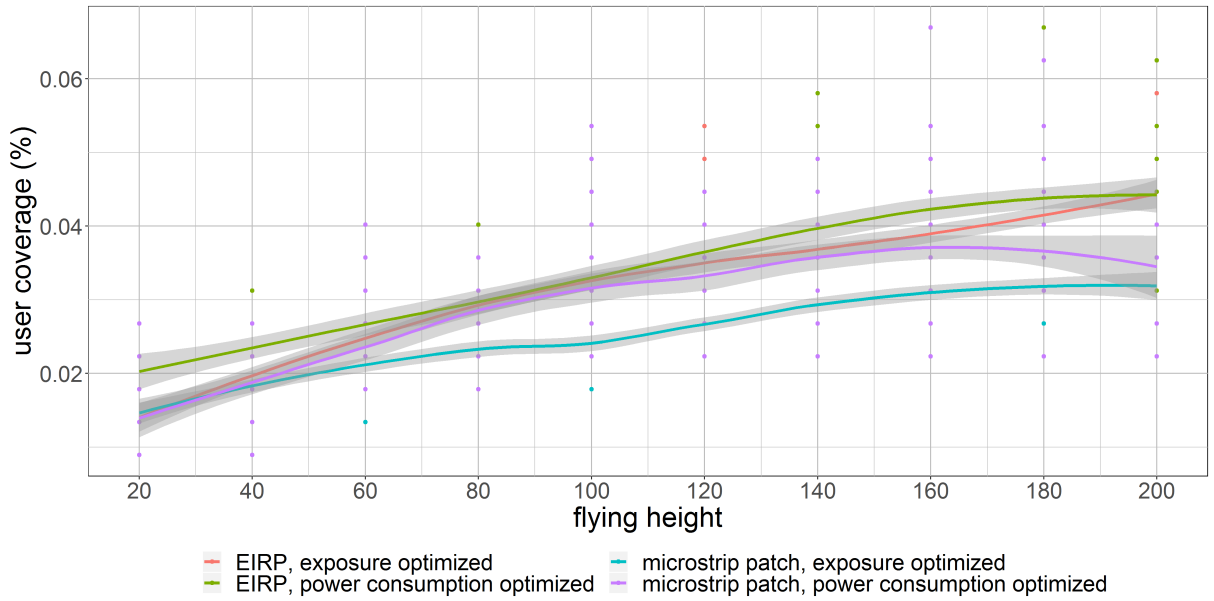


Figure 5.7: This graph shows the percentage of covered users by one drone for different flying heights.

Chart 5.8 shows the whole body SAR10g, deducted from all electromagnetic sources. This being exposure of all UABSs, the uplink exposure from the user's own device and the exposure of the devices from all other users. Thereafter, the weighted average of all whole body SAR10g values in the network is calculated with the 50th and 95th percentile being the most important values. This is because not only the mean values are important but also users who experience higher levels of whole body SAR10g.

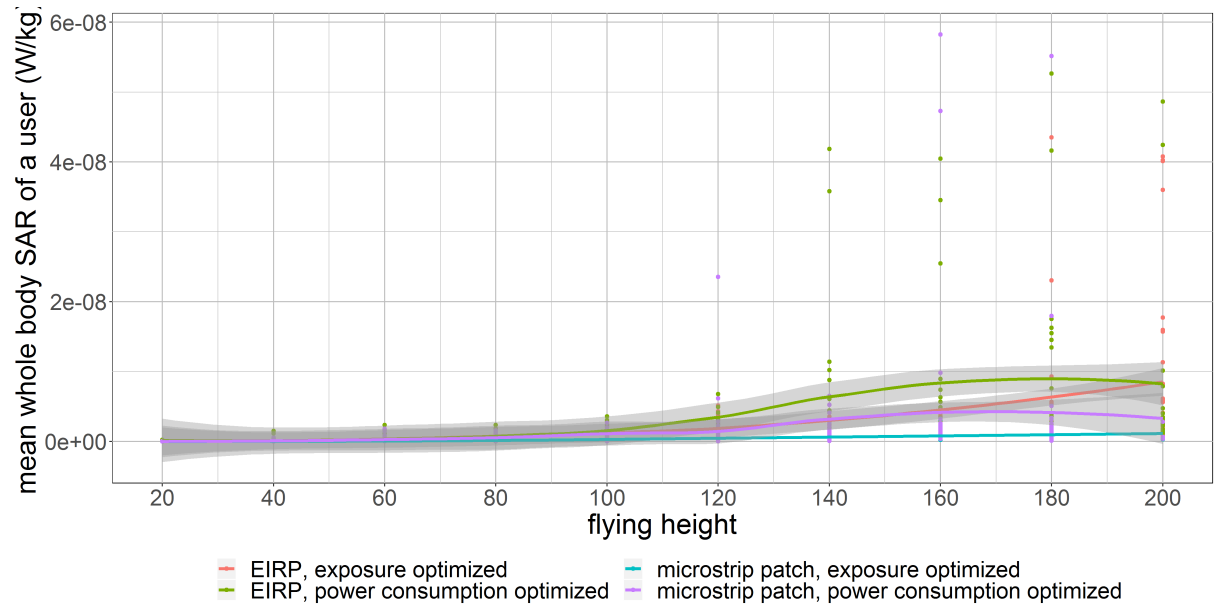


Figure 5.8: The influence of the flying height on the weighted average  $SAR_{10g}$  of users in the network.

When investigating the 3 different sources for the total SAR-values from 5.8, we see that the radiation from all different UABSs is the main factor followed by the near field radiation from the user's own device. The far field radiation from other UE has barely influence. It looks like it is zero but it is just very low compared to the other two values.

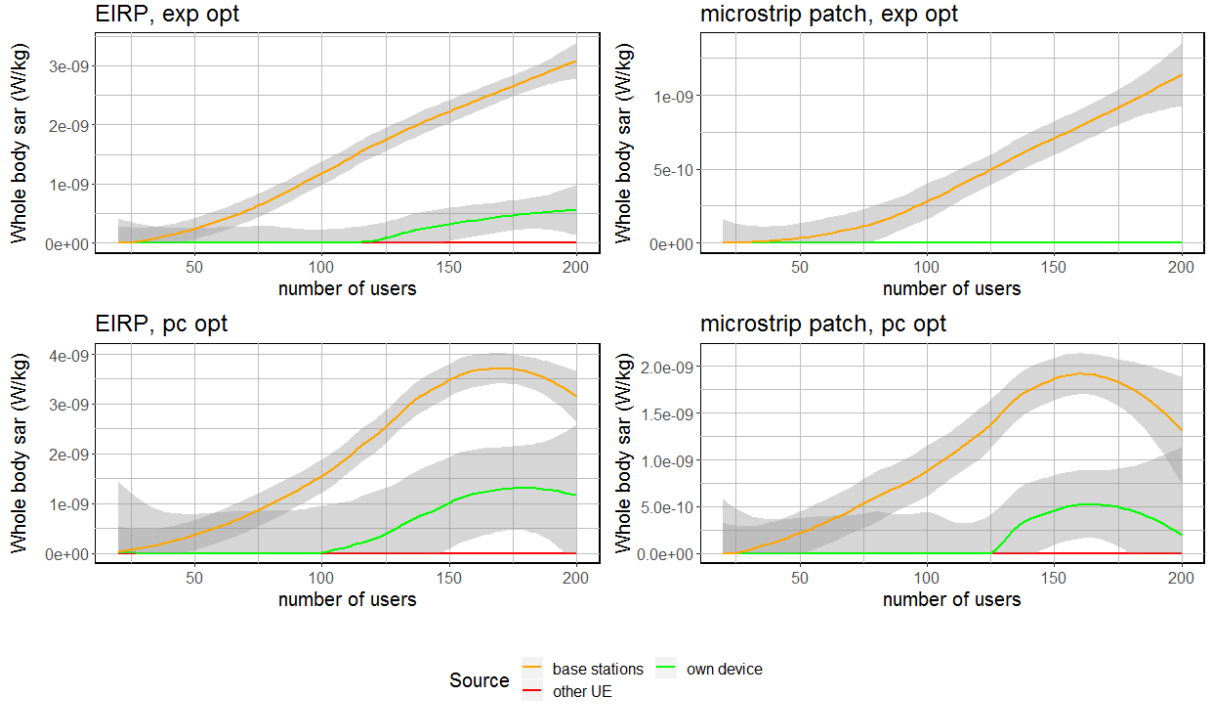


Figure 5.9: This figure shows how different sources are influenced by an increasing flying height.

### 5.2.2 Influence of the number of users

The number of covered users increase linearly compared to the number of users present in the network. An equivalent isotropic radiator has no attenuation and is therefore able to reach more users. On the other side, an power consumption optimized network with only one drone will result in a high powered UABS as explained before and is therefore also able to cover more users. The complete opposite is a microstrip patch in an exposure optimized network (which is the blue line in figure 5.10) and covers the least number of users.

The linear regression lines from 5.10 can be predicted with the equations in 5.2.

$$\text{number of users} = \begin{cases} y = 0,0233x + 2,3553 & \text{if EIRP and pc} \\ y = 0,0197x + 2,6144 & \text{if EIRP and exp} \\ y = 0,0131x + 2,4371 & \text{if micro and pc} \\ y = 0,0119x + 2,4652 & \text{if micro and exp} \end{cases} \quad (5.2)$$

The percentage of covered users is achieved by taking the equations from 5.2 and dividing them by  $x$ . Figure 5.11 shows a decreasing logarithmic behaviour because the regression lines from 5.10 have a slope of less than 0.5. So in other words, the percentage of covered users for a sparsely

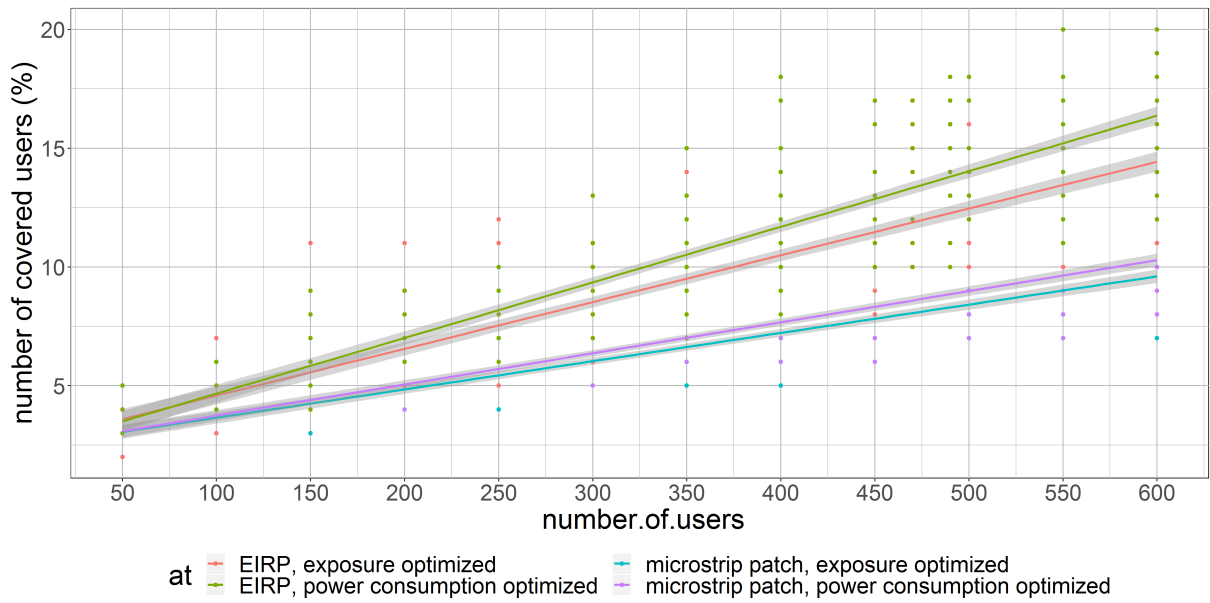


Figure 5.10: The influence of increasing traffic on user coverage

populated network is more compared to the percentage of users in high dense populations.

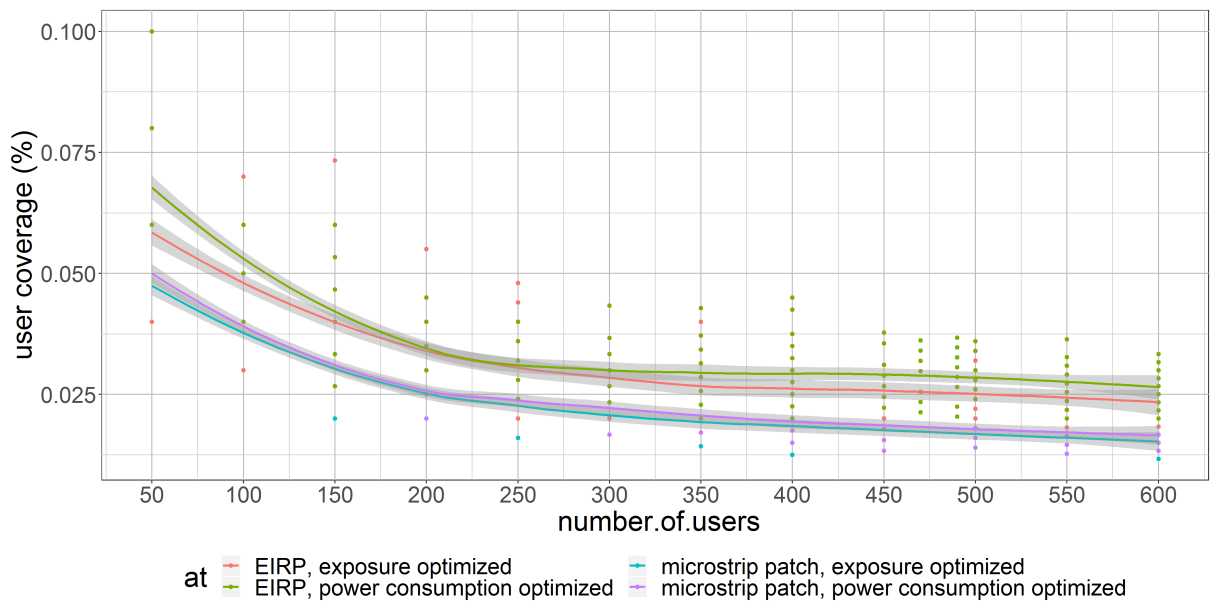


Figure 5.11: The influence of increasing traffic on user coverage

The downlink exposure is directly influenced by the number of covered users (figure 5.12). The electromagnetic exposure increases when more users are covered and since an equivalent isotropic radiator in a power consumption optimized network (green) will have the highest coverage, also the D/L electromagnetic radiation from UABSs will be higher.

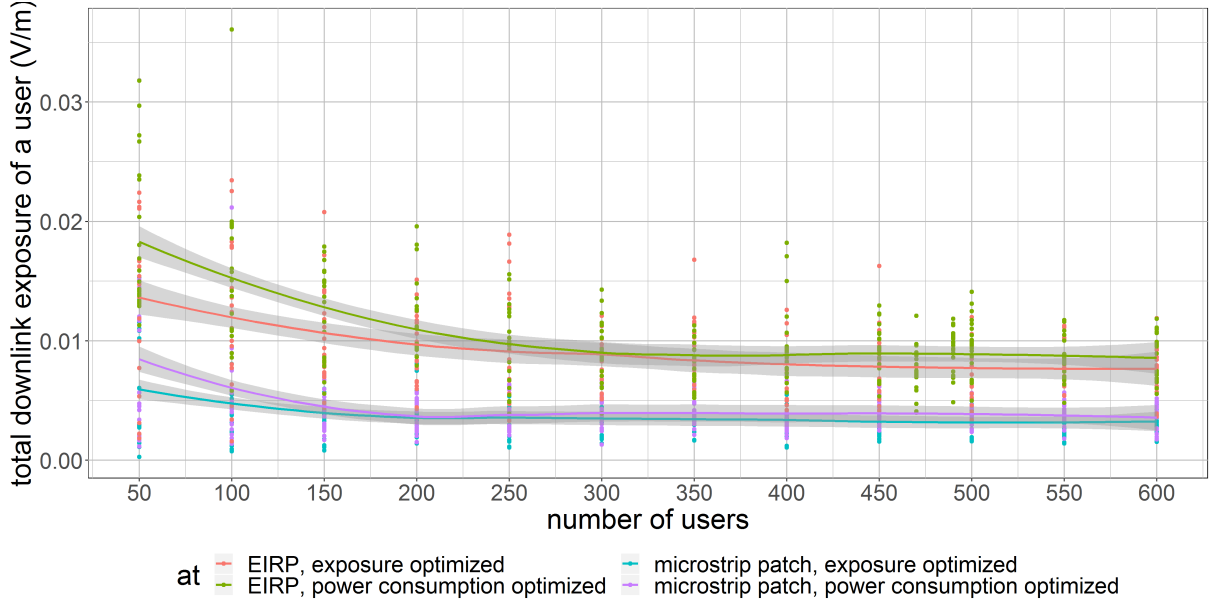


Figure 5.12: The influence of increasing traffic on downlink exposure

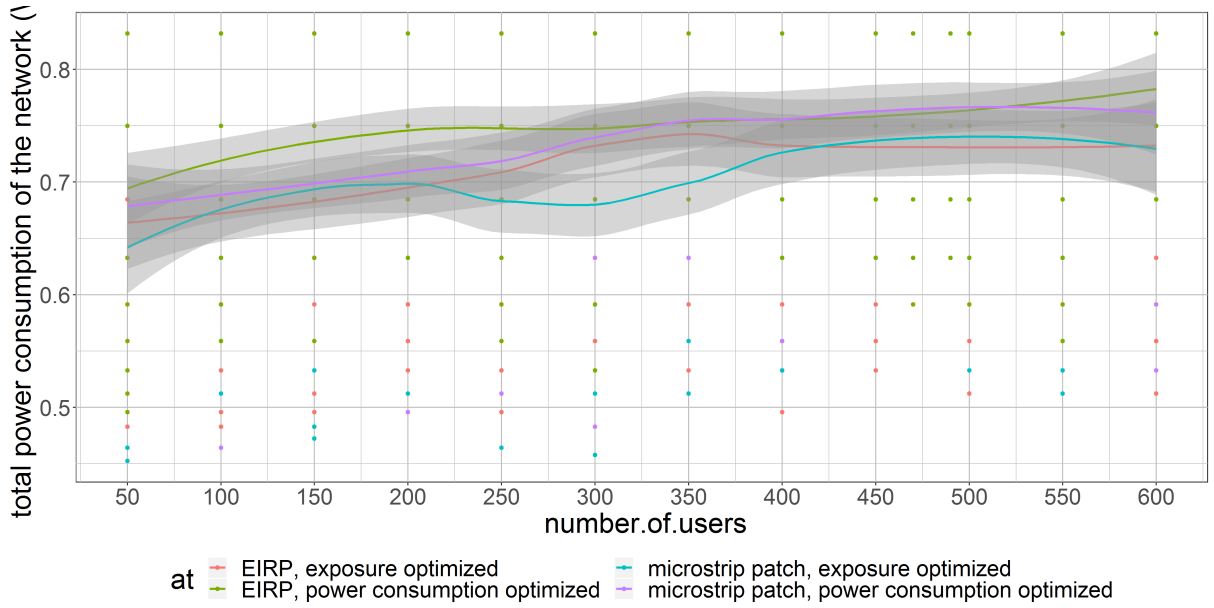


Figure 5.13: The influence of increasing traffic on the total power consumption

The optimization strategies only consider D/L exposure and power consumption. However, how much radiation is absorbed by the users originating from all sources is shown in ?? and the relative position of the four configurations do not differ compared to the ??. So an D/L exposure optimized network with an equivalent isotropic radiator which result in the highest electromagnetic exposure for this scenario will also have the highest specific absorption rate according to figure 5.14. The same applies for the other configurations as well.

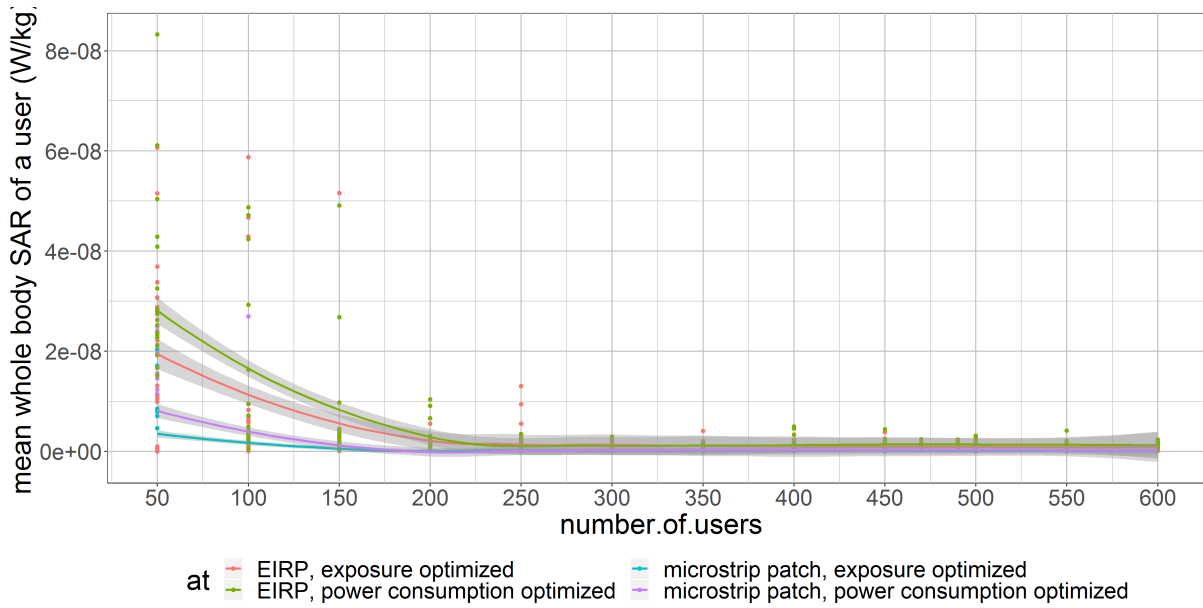


Figure 5.14: This figure shows how different sources are influenced by an increasing number of users.

Figure 5.15 investigates the assets of each source to the SAR. All four configuration show that for 200 users and up, base stations are the main source of electromagnetic radiation.

For less users, the electromagnetic radiation from the user's device is much higher. Chart 5.11 already showed that for 200 users and less, the number of covered user's is higher but there is still only one UABS available. So UE need to radiate much more in order to still be able to reach that one drone.

The red line proves that the far field electromagnetic exposure from other users their device can be neglected. The SAR from neighbouring devices is not zero as it looks from figure 5.15 but is just really low compared to the much higher SAR-values from other sources.

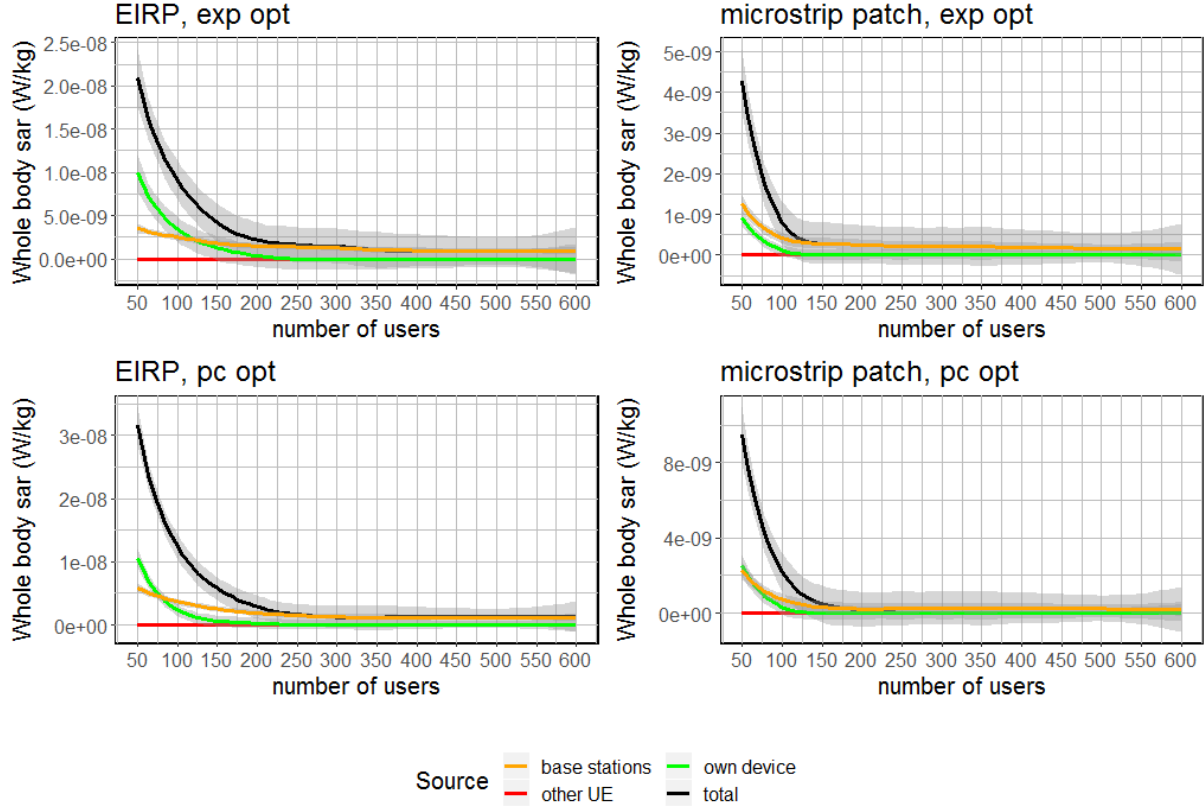


Figure 5.15: This figure shows how different sources are influenced by an increasing number of users.

### 5.3 Scenario 3:

#### 5.3.1 Influence of the flying altitude

This scenario examines the same cases as scenario 2 but there is no restriction on the number of UABSs. Unlike in scenario 2, fig. 5.16 and 5.19 show a clearer view on how the decision algorithms works. Antennae in an exposure optimized network cause less downlink exposure (fig. 5.16). On the other hand, a network generated for optimal power consumption requires indeed less energy as proven in figure 5.19.

Figure 5.16 shows how an equivalent isotropic radiator in and power consumption optimized network has the highest exposure when the UABS is close to the ground. An power consumption optimized network results in less number of drones which can also be seen on figure ???. The network is still trying to cover as much users as possible as visible on figure 5.18 (with in this case less resources). Low flying drones need to account for increased path loss by obstructing buildings. When the flying altitude increases, there is less path loss and the electromagnetic



exposure stabilizes. The same is applicable when replacing the equivalent isotropic radiator with a microstrip patch antenna but users will experience less electromagnetic radiation because of antenna aperture. Because the algorithm still tries to cover as much users as possible, the tool will react to this by introducing more drones (fig ??).

When changing the optimization strategy towards an exposure optimized network, the lowest possible electromagnetic radiation is recorded with low flying drones at 20 m height with microstrip patch antennae. Using an equivalent isotropic radiator automatically increases electromagnetic radiation because of the absence of attenuation. This behaviour results in an higher necessity of antenna carriers ??.

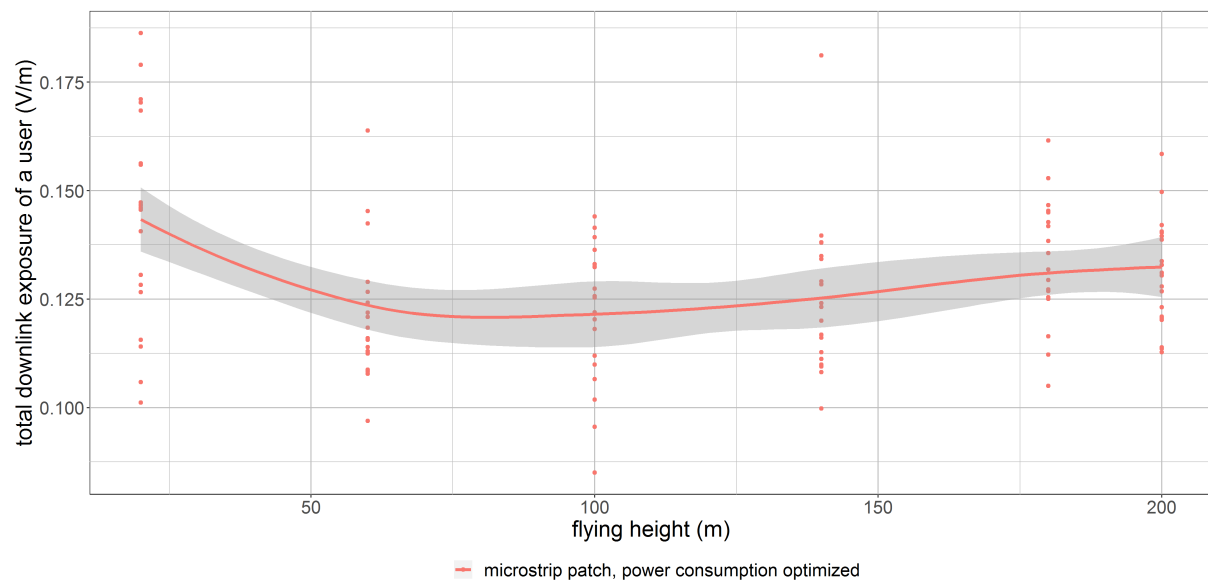


Figure 5.16: The influence of the flying height on the downlink electromagnetic radiation of the average user.

Both ?? and 5.19 show that the network profit from increasing the flying altitude. Not only less drones are needed but also the power consumption is lower. Both can be explained by the lower path loss when UABSs fly higher. If a user cannot be covered because an UABSs is too far away or is saturated with other users, the tool can simply add another UABS. The only remaining reason that a user can't be covered is because the position of the drone is obstructed by a building. The higher drones fly, the less change the position is obstructed by a building. In gent is this chance is zero when flying higher then 119 meters. Since the 'Artevelde Tower' is the highest building in Ghent.

Scenario 1 already proved that with low flying drones, the main source of electromagnetic radiation are UABS. This changes around 80 meters where U/L electromagnetic radiation of the UE exceeds D/L radiation in order to still be able to reach the high flying UABSs.

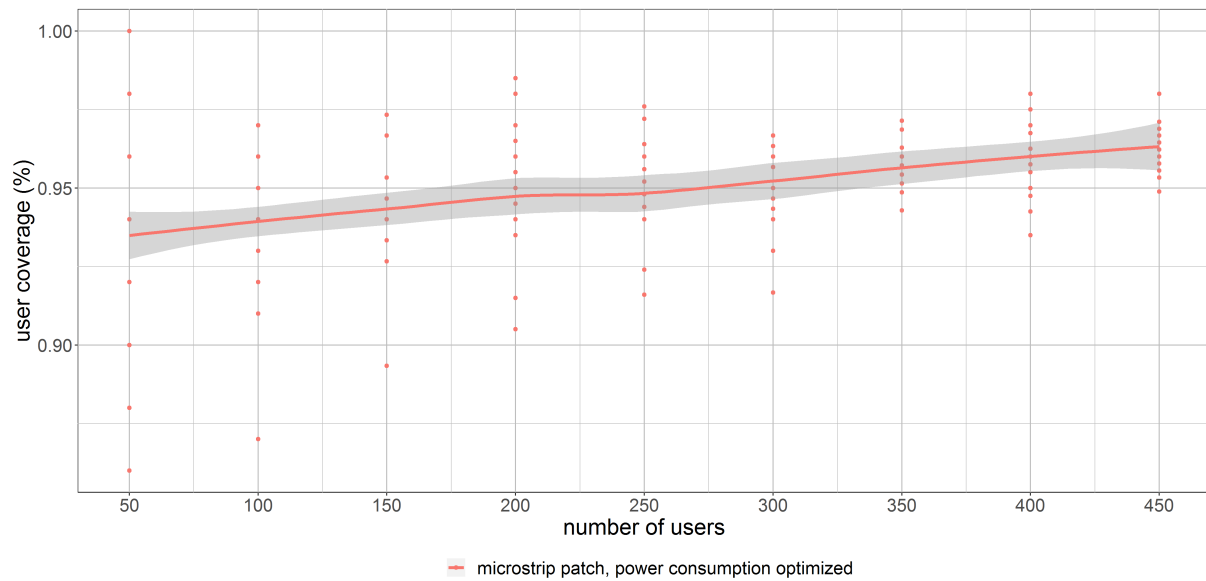


Figure 5.17: This graph shows the percentage of covered users by one drone for different flying heights.

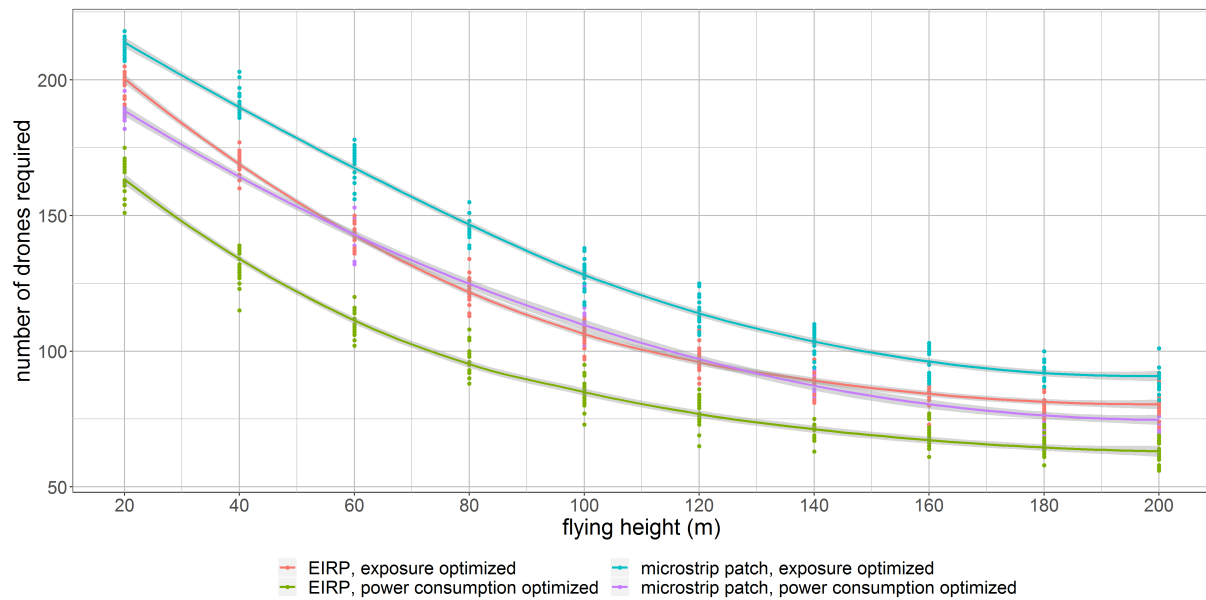


Figure 5.18: This graph shows how much drones are required for different flying heights while trying to achieve a 100% coverage.

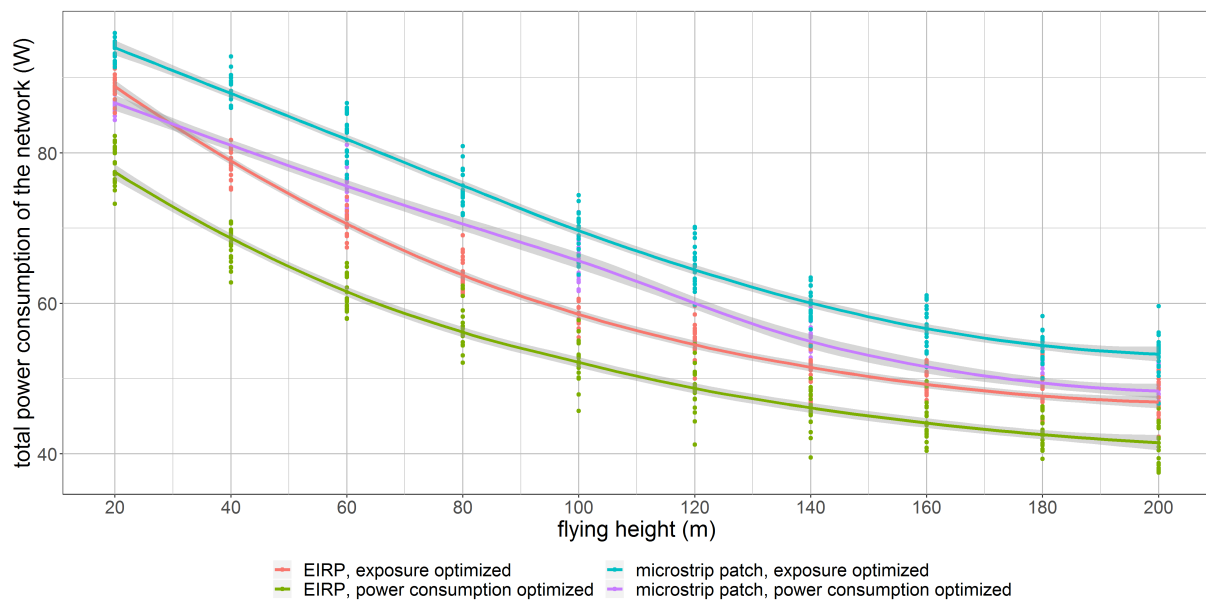


Figure 5.19: The influence of the flying height on the total power consumption of the network.

### 5.3.2 Influence of the number of users

todo

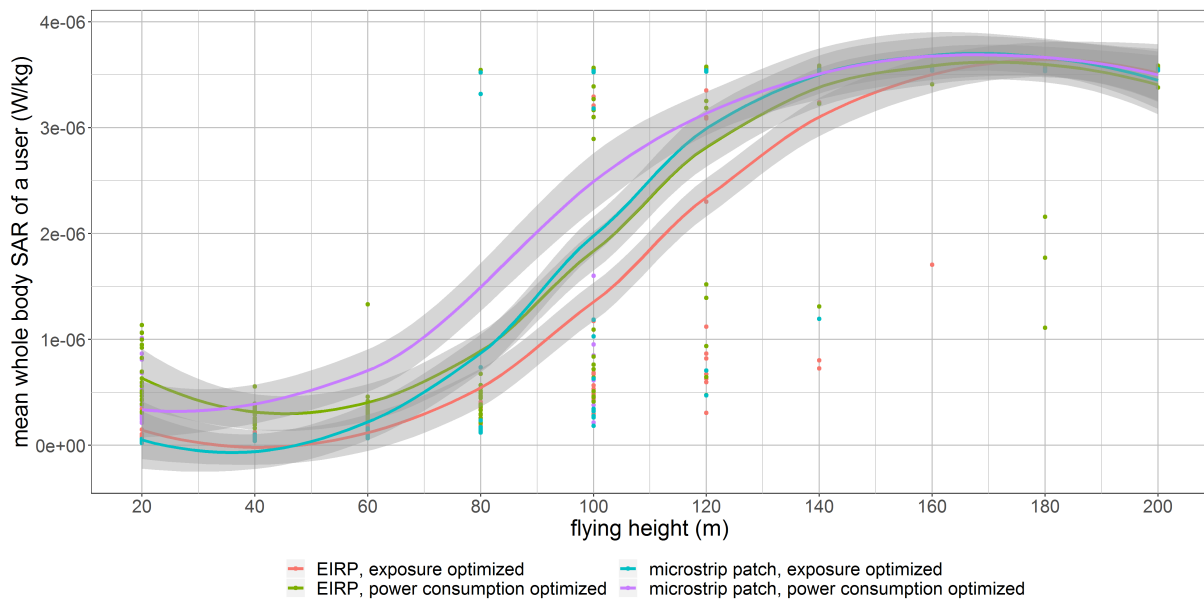


Figure 5.20: The influence of the flying height on the weighted average  $SAR_{10g}$  of users in the network.

# 6

## Conclusions

todo

far field radiation from UE has barely influence on the total SAR. For simplified models, this factor can be ignored.

## Bibliography

- [1] “kaart van mobiel netwerkbereik.” <https://www.test-aankoop.be/hightech/gsms-en-smartphones/module/kaart-van-mobiel-netwerkbereik>. Accessed: 03-03-2020.
- [2] D. standaard, “Base overschreed stralingsnormen na aanslagen,” *De standaard*, 2016.
- [3] L. Hardell and C. Sage, “Biological effects from electromagnetic field exposure and public exposure standards,” *Biomedicine and Pharmacotherapy*, vol. 62, no. 2, pp. 104 – 109, 2008.
- [4] “Electromagnetic fields (emf),” Nov.
- [5] M. Deruyck, J. Wyckmans, W. Joseph, and L. Martens, “Designing uav-aided emergency networks for large-scale disaster scenarios,” *EURASIP Journal on Wireless Communications and Networking*, vol. 2018, 12 2018.
- [6] v. v. d. v. e. l. Federale overheidsdienst: volksgezondheid, “Elektromagnetische velden en gezondheid: Uw wegwijzer in het elektromagnetische landschap,” vol. 5, 2014.
- [7] I. Guideline, “Guidelines for limiting exposure to time-varying electric, magnetic, and electromagnetic fields (up to 300 ghz),” *Health phys*, vol. 74, no. 4, pp. 494–522, 1998.
- [8] D. Plets, W. Joseph, K. Vanhecke, and L. Martens, “Exposure optimization in indoor wireless networks by heuristic network planning,” *Progress In Electromagnetics Research*, vol. 139, pp. 445–478, 01 2013.
- [9] M. Deruyck, E. Tanghe, D. Plets, L. Martens, and W. Joseph, “Optimizing lte wireless access networks towards power consumption and electromagnetic exposure of human beings,” *Computer Networks*, vol. 94, 12 2015.
- [10] D. Plets, W. Joseph, S. Aerts, K. Vanhecke, G. Vermeeren, and L. Martens, “Prediction and comparison of downlink electric-field and uplink localised sar values for realistic indoor wireless planning,” *Radiation Protection Dosimetry*, vol. 162, no. 4, pp. 487–498, 2014.
- [11] D. Plets, W. Joseph, K. Vanhecke, and L. Martens, “Downlink electric-field and uplink sar prediction algorithm in indoor wireless network planner,” in *The 8th European Conference on Antennas and Propagation (EuCAP 2014)*, pp. 2457–2461, IEEE, 2014.

- [12] S. Kuehn, S. Pfeifer, B. Kochali, and N. Kuster, "Modelling of total exposure in hypothetical 5g mobile networks for varied topologies and user scenarios," *Final Report of Project CRR-816*, Available on line at: <https://tinyurl.com/r6z2gqn>, 2019.
- [13] D. Plets, W. Joseph, K. Vanhecke, G. Vermeeren, J. Wiart, S. Aerts, N. Varsier, and L. Martens, "Joint minimization of uplink and downlink whole-body exposure dose in indoor wireless networks," *BioMed research international*, vol. 2015, 2015.
- [14] I. Singh and V. Tripathi, "Micro strip patch antenna and its applications: a survey," *Int. J. Comp. Tech. Appl*, vol. 2, no. 5, pp. 1595–1599, 2011.
- [15] K. Kashwan, V. Rajeshkumar, T. Gunasekaran, and K. S. Kumar, "Design and characterization of pin fed microstrip patch antennae," in *2011 Eighth International Conference on Fuzzy Systems and Knowledge Discovery (FSKD)*, vol. 4, pp. 2258–2262, IEEE, 2011.
- [16] I. Singh and V. Tripathi, "Micro strip patch antenna and its applications: a survey," *Int. J. Comp. Tech. Appl*, vol. 2, no. 5, pp. 1595–1599, 2011.
- [17] A. Sudarsan and A. Prabhu, "Design and development of microstrip patch antenna," *International Journal of Antennas (JANT) Vol*, vol. 3, 2017.
- [18] A. Christ, M.-C. Gosselin, M. Christopoulou, S. Kühn, and N. Kuster, "Age-dependent tissue-specific exposure of cell phone users," *Physics in Medicine & Biology*, vol. 55, no. 7, p. 1767, 2010.
- [19] P. Joshi, D. Colombi, B. Thors, L.-E. Larsson, and C. Törnevik, "Output power levels of 4g user equipment and implications on realistic rf emf exposure assessments," *IEEE Access*, vol. 5, pp. 4545–4550, 2017.
- [20] "Bundesamt für strahlenschutz." [http://www.bfs.de/SiteGlobals/Forms/Suche/BfS/EN/SARsuche\\_Formular.html](http://www.bfs.de/SiteGlobals/Forms/Suche/BfS/EN/SARsuche_Formular.html). Accessed: 14-10-2019.
- [21] A. Gati, E. Conil, M.-F. Wong, and J. Wiart, "Duality between uplink local and downlink whole-body exposures in operating networks," *IEEE transactions on electromagnetic compatibility*, vol. 52, no. 4, pp. 829–836, 2010.

# Appendices





## Radiation patterns: datasheet

Table A.1 gives an overview of the attenuation in the E and H plane. The first radiation pattern is with a square groundplane with an edge of 0.060 meter while the second pattern is more of a rectangular shape with a width of 0.0524m and a lenght of 0.0438m. All other settings are equal as defined in 4.1.4

Table A.1: Overview of attenuation in dBm

	pattern 1		pattern 2	
angle	E	H	E	H
0	0,00	0,00	0	0
10	-0,17	-0,14	-0.1561	-0.158
20	-0,67	-0,57	-0.5797	-0.6257
30	-1,48	-1,27	-1.263	-1.386
40	-2,57	-2,22	-2.193	-2.412
50	-3,90	-3,39	-3.357	-3.665
60	-5,40	-4,73	-4.741	-5.099
70	-7,09	-6,23	-6.337	-6.658
80	-8,82	-7,87	-8.136	-8.278
90	-10,54	-9,70	-10.11	-9.88
100	-12,20	-11,84	-12.14	-11.34
110	-13,73	-14,37	-13.81	-12.47
120	-15,04	-17,65	-14.42	-13.00
130	-16,01	-21,83	-13.72	-12.82
140	-16,47	-23,63	-12.41	-12.08
150	-16,42	-20,37	-11.15	-11.15
160	-16,05	-17,49	-10.21	-10.33
170	-15,69	-15,93	-9.683	-9.786
180	-15,54	-15,54	-9.596	-9.596
190	-15,69	-16,30	-9.963	-9.784
200	-16,05	-18,44	-10.79	-10.33
210	-16,42	-22,85	-12.07	-11.15
220	-16,47	-31,23	-13.71	-12.07
230	-16,00	-24,07	-15.25	-12.80
240	-15,03	-18,05	-15.65	-12.99
250	-13,72	-14,42	-14.3	-12.45
260	-12,20	-11,81	-12.11	-11.33
270	-10,54	-9,70	-9.882	-9.866
280	-8,82	-7,87	-7.859	-8.267
290	-7,09	-6,23	-6.069	-6.649
300	-5,40	-4,73	-4.502	-5.093
310	-3,90	-3,39	-3.154	-3.661
320	-2,57	-2,22	-2.029	-2.409
330	-1,48	-1,27	-1.138	-1.384
340	-0,67	-0,57	-0.4963	-0.6246
350	-0,17	-0,14	-1143	-0.1575



## Radiation patterns: example configuration

In listing 2 is a possible configuration described for a radiation pattern. It is important to notice that this example configuration does not represent the used configuration in this master dissertation. The `radiationPattern`-tag consist of a `slices`-tag. This tag can contain as much slices as desired. In this example, 3 slices are defined indicated with the `attenuation`-tag. This tag contains a mandatory attribute `az` which defines the azimuth angle to which all underlying attenuation values belong. Inside the `attenuation`-tag are all attenuation values written in a `value`-tag.

The tool distributes all values equally over the  $180^\circ$  of that slice. In the example below, each `attenuation`-tag contains 10 values meaning that the exact attenuation is known every  $20^\circ$ .

The highlighted value of -14,42 is therefore measured at an azimuth angle of  $0^\circ$  and an elevation angle of  $120^\circ$  (counterclockwise).

```

1  <radiationPattern>
2    <slices>
3      <attenuation az="0">
4        <value>0</value>
5        <value>-0.5797</value>
6        <value>-2.193</value>
7        <value>-4.741</value>
8        <value>-8.136</value>
9        <value>-12.14</value>
10       <value>-14.42</value>
11       <value>-12.41</value>
12       <value>-10.21</value>
13       <value>-9.596</value>
14     </attenuation>
15     <attenuation az="90">
16       <value>0</value>
17       <value>-0.6257</value>
18       <value>-2.412</value>
19       <value>-5.099</value>
20       <value>-8.278</value>
21       <value>-11.34</value>
22       <value>-13.00</value>
23       <value>-12.08</value>
24       <value>-10.33</value>
25       <value>-9.596</value>
26     </attenuation>
27     <attenuation az="180">
28       <value>0</value>
29       <value>-0.4963</value>
30       <value>-2.029</value>
31       <value>-4.502</value>
32       <value>-7.859</value>
33       <value>-12.11</value>
34       <value>-15.65</value>
35       <value>-13.71</value>
36       <value>-10.79</value>
37       <value>-9.596</value>
38     </attenuation>
39   </slices>
40 </radiationPattern>

```

Listing 2: Example configuration of a radiation pattern.